



# Cold-water coral mounds are effective carbon sinks in the western Mediterranean Sea

Luis Greiffenhagen<sup>1</sup>, Jürgen Titschack<sup>1</sup>, Claudia Wienberg<sup>1</sup>, Haozhuang Wang<sup>1,2</sup>, and Dierk Hebbeln<sup>1,3</sup>

<sup>1</sup>MARUM – Center for Marine Environmental Sciences, University of Bremen, Bremen, Germany

<sup>2</sup>State Key Laboratory of Marine Geology, Tongji University, Shanghai, China

<sup>3</sup>Faculty of Geosciences, University of Bremen, Bremen, Germany

**Correspondence:** Luis Greiffenhagen (lgreiffenhagen@marum.de)

Received: 11 August 2024 – Discussion started: 2 October 2024

Revised: 4 February 2025 – Accepted: 10 February 2025 – Published: 9 May 2025

**Abstract.** Cold-water corals (CWCs) build biogenic structures, known as CWC mounds, that can store large amounts of carbon(ate). However, there is a lack of quantification studies on both recent as well as geological timescales, and knowledge is limited to the accumulation of carbonate (i.e. the inorganic carbon fraction), which ignores the organic carbon fraction. This hinders the calculation of total carbon accumulation rates and a wider understanding of the role CWC mounds play in the carbon cycle. Here, we investigated two cores retrieved from CWC mounds in the Alborán Sea, western Mediterranean Sea, comprising a  $\sim 400$  kyr record of carbon accumulation. We calculated the accumulation of both inorganic and organic carbon within the CWC mounds. Further, we analysed the same parameters in two cores from the adjacent seafloor ( $\sim 120$  kyr record) to compare the mound records with the surrounding sedimentary deposits. Our results show that the CWC mounds studied accumulate up to  $15 \text{ g C cm}^{-2} \text{ kyr}^{-1}$ , of which 6%–9% is derived from the organic carbon fraction. Moreover, during mound formation phases, the mounds store up to 14–19 times more carbon than the adjacent seafloor deposits. We suggest that there is a selective enrichment of organic carbon on the mounds, with about an order of magnitude higher organic carbon accumulation rates than on the adjacent seafloor. Consequently, in phases of mound formation, CWC mounds can be effective local sinks of both inorganic and organic carbon on geological timescales.

## 1 Introduction

Within the carbon cycle, there are two subcycles, the short-term and the long-term carbon cycle (Burdige, 2007; Cartapanis et al., 2018). Within the world's oceans, the bulk of carbon stays in the “active” short-term cycle, while a small fraction is buried in the sediment that gets removed from the active system and transferred to the geological inventory (the long-term carbon cycle; Cartapanis et al., 2018). This fraction is immobilised for millions of years and stored as organic carbon ( $C_{\text{org}}$ ) or inorganic carbon ( $C_{\text{inorg}}$ , i.e. derived from calcium carbonate). Benthic carbonate production through calcification plays a major role in this process (Ridgwell and Zeebe, 2005). As carbonate factories, some calcifying organisms create biogenic structures or extensive carbonate-rich facies over thousands of years (Schlager, 2000, 2003; Reijmer, 2021). Their carbonate accumulation has been quantified (Milliman, 1974, 1993; Smith and Mackenzie, 2016; O'Mara and Dunne, 2019); however, large knowledge gaps and high uncertainties remain (Cartapanis et al., 2018; Michel et al., 2019; Wood et al., 2023), especially for cold-water carbonate factories. In this context, cold-water coral (CWC) reefs in the deep sea may also play a significant role in the marine carbon budget (e.g. Lindberg and Mienert, 2005; Titschack et al., 2015; Hebbeln et al., 2019; Reijmer, 2021). However, due to the particular technological difficulty of exploring CWC reefs (mostly at 200–1200 m water depth), knowledge about their overall role in the marine carbonate budget is still limited. CWCs occur circumglobally, with only a few scleractinian CWCs, i.e. carbonate-framework-forming corals such as *Lophelia pertusa* (syn. *Desmophyllum pertusum*) and *Madrepora ocu-*

*lata*, being capable of building entire CWC reefs (Roberts et al., 2009; Wienberg and Titschack, 2017). With their three-dimensional framework, these CWCs provide the habitat and the foundation for some of the most biodiverse ecosystems of the deep sea (Henry and Roberts, 2007, 2017). The occurrence and proliferation of CWC reefs depend on a certain range of environmental conditions, such as temperature, pH, and oxygenation (e.g. Davies and Guinotte, 2011), combined with a sufficient nutrient supply through bottom currents and primary production (e.g. Portilho-Ramos et al., 2022; Maier et al., 2023).

In millennial-scale cycles of proliferation and extinction (e.g. Dorschel et al., 2005; Roberts et al., 2009; Wienberg and Titschack, 2017), CWC reefs build “CWC mounds”, consisting of successive generations of carbonate-framework-forming corals that grow on top of each other and are stabilised by sediment infill (e.g. de Haas et al., 2009; Titschack et al., 2009; Wang et al., 2021). Individual periods of reef proliferation are herein referred to as “mound formation phases”. The investigation of sediment cores taken from CWC mounds revealed that during mound formation phases, large amounts of carbonate accumulate (e.g. Dorschel et al., 2007b; Titschack et al., 2009). Thereby, one part is derived from the coral carbonate itself, and the other part comes from pelagic and benthic carbonate buried within the sediment that significantly contributes to mound formation (e.g. Titschack et al., 2009). High-resolution 3D-imagery-based core studies provide evidence that CWC mounds are substantial carbonate sinks, when comparing their accumulation rates to the surrounding sedimentary environments (Titschack et al., 2015, 2016). Moreover, the accumulation rates from CWC mounds are in the same range as other regional carbonate factories such as coralline algal beds, tropical warm-water coral reefs, and bryozoan facies (Titschack et al., 2016). Spatially upscaled estimates of carbonate accumulation for an entire mound province suggest significant regional or potentially global importance (Titschack et al., 2009; Hebbeln et al., 2019; Tamborrino et al., 2022).

Due to the limited number of published carbonate accumulation rates (ranging from 0.3 to 2114 g CaCO<sub>3</sub> cm<sup>-2</sup> kyr<sup>-1</sup>) for CWC mounds over both time and space (Lindberg and Mienert, 2005; Dorschel et al., 2007b; Titschack et al., 2009, 2015, 2016; Edinger et al., 2025), CWC mounds are still not a part of global carbon(ate) budget calculations – or at least are not well-represented (Titschack et al., 2015; Smith and Mackenzie, 2016; Wood et al., 2023). Existing high-resolution studies (Titschack et al., 2015, 2016) focus on the most recent mound formation phase. Hence, the detailed variation in carbonate accumulation across multiple mound formation phases remains unknown. Further, all studies so far have focused on the carbonate fraction (i.e. C<sub>inorg</sub>) of the carbon accumulation on CWC mounds, and there is no study that combines C<sub>inorg</sub> with C<sub>org</sub> to get the holistic total mound carbon accumulation.

Here, we investigated ~400 000 years of CWC mound formation in the Alborán Sea, western Mediterranean. Covering seven mound formation phases, we quantify the accumulation of C<sub>inorg</sub> and C<sub>org</sub> from two CWC mounds (based on two coral-bearing sediment cores) and provide the first total carbon accumulation rates. To provide evidence for their local significance in the long-term carbon cycle and as potential sinks of C<sub>inorg</sub> and C<sub>org</sub>, we further compare these rates with those obtained from the adjacent seafloor (based on coral-barren sediment cores).

## 2 Regional setting

Within the Mediterranean Sea, the Alborán Sea is a hotspot of primary productivity (Morán and Estrada, 2001; Sánchez-Garrido and Nadal, 2022); CWC mound formation (Lo Iacono et al., 2014; Stalder et al., 2018; Corbera et al., 2019; Hebbeln, 2019; Wang et al., 2019; Wienberg, 2019; Corbera et al., 2021; Wienberg et al., 2022); and, potentially, carbon burial (Masqué et al., 2003). The presence of CWCs in the Alborán Sea is closely linked to the flow path of the Levantine Intermediate Water (LIW) (Hayes et al., 2019). This well-ventilated and nutrient-rich water mass (Álvarez et al., 2023) promotes primary production as well as oxygen and food supply to the CWCs living on the mounds (Wienberg et al., 2022). In addition, the steep density gradient (pycnocline) between the low-salinity LIW and the high-salinity overlying Atlantic Water (Millot, 1999) can be disturbed when it intersects sloping topography, resulting in the formation of high-energy internal waves (e.g. Ercilla et al., 2016) that further enhance the delivery of food particles. In the southern Alborán Sea off the Moroccan margin lies the East Melilla Coral Province (EMCP), which comprises various CWC mounds of very different sizes and morphologies rising from water depths of 210–475 m on the upper continental slope (Fig. 1; Hebbeln, 2019). The CWC mounds of the EMCP developed during multiple mound formation phases from (at least) marine isotope stage (MIS) 11 (~390 kyr ago) up to the early Holocene. Mound formation phases in the EMCP correspond mainly to interglacial periods but also to one glacial period (MIS 10). While there is no clear link between phases of active CWC mound formation and ice-age-paced climate oscillations, there seems to be a strong coupling with changes in the African hydroclimate (see Wienberg et al., 2022, for a detailed description).

## 3 Material and methods

This study focuses on four sediment cores collected from the EMCP in the Alborán Sea (Table 1). Two cores are taken from the CWC mounds Brittlestar Ridge I (BRI) and Dragon Mound (the on-mound cores GeoB18116-2 and GeoB13729-1) and two from the same location in the “off-mound” area between the mounds (the off-mound cores MD13-3457 and

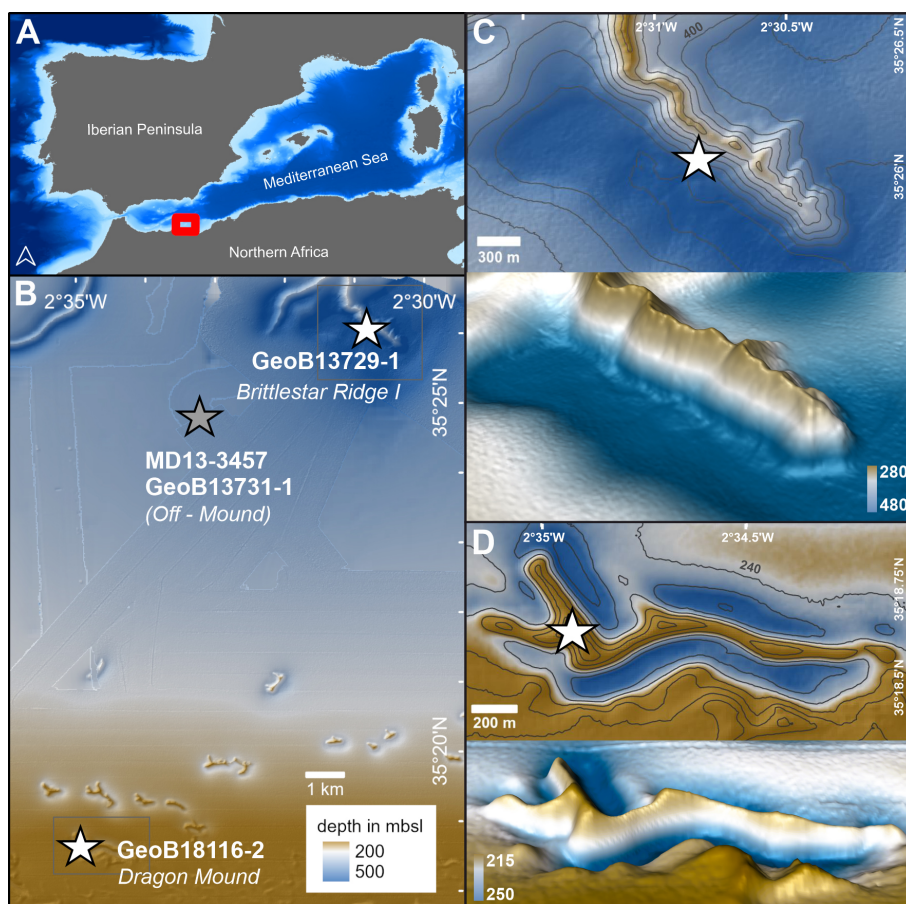


**Figure 1.** (a) The study area (red box) located within the western Mediterranean Sea. (b) The East Melilla Coral Province (EMCP, red box in a) showing the location of sediment cores (stars, white represents mound cores, and grey represents off-mound cores) used in this study. (c) Close up view of Brittlestar Ridge I, with 2D (contour lines every 25 m of depth) and 3D views (3× vertical exaggeration). (d) Close up view of Dragon Mound, with 2D (contour lines every 5 m of depth) and 3D views (7.5× vertical exaggeration). Maps created using ESRI ArcGIS Pro and ZIB Amira software. Bathymetry data derived from the GEBCO Bathymetric Compilation Group (2024, in a) and partly supplemented by EMODnet Bathymetry Consortium (2022, in b). A detailed bathymetry of the EMCP is available at <https://doi.org/10.1594/PANGAEA.895349> (Hebbeln and Gaide, 2018).

GeoB13731-1; Fig. 1). Brittlestar Ridge I, located in the northern part of the EMCP, is an elongated, ridge-shaped CWC mound with a height of 140 m above the seabed, while the much smaller and shallower Dragon Mound situated ~ 15 km to the south of BRI rises 20–30 m above the seafloor (Fig. 1), with a 30–40 m extension below the seafloor.

The on-mound core GeoB18116-2 was taken during the R/V *Maria S. Merian* cruise MSM36 “MoccoMeBo” (Hebbeln et al., 2015) using the seafloor drill rig MeBo70 from MARUM, University of Bremen, Germany (Freudenthal and Wefer, 2013). The ~ 70 m long MeBo core was retrieved from the summit of Dragon Mound in the southern part of the EMCP (Fig. 1, Table 1; Wienberg et al., 2022, for more details). MeBo drill cores are recovered in core barrels (235 cm each), which may lack sediment material (i.e. gaps in the sedimentary units) due to drilling operations or may have recoveries > 100 % due to core expansion (this needs to

be corrected for using specific depth models; see Sect. 3.2). Overall, GeoB18116-2 has a recovery rate of 96 % and contains coral fragments down to a core depth of ~ 60–61 m (encompassing 26 core barrels), while below, only fine-grained coral-barren sediments occur (Wienberg et al., 2022). Completely penetrating a large CWC mound from the top to its base, GeoB18116-2 is a unique record in the Mediterranean Sea. Its corresponding stratigraphy covers an approximate time span between ~ 100 and 390 kyr BP and includes several mound formation phases (~ MIS5–MIS11; Wienberg et al., 2022).

The on-mound core GeoB13729-1 was collected from BRI during the R/V *Poseidon* cruise POS385 (Fig. 1; Hebbeln et al., 2009). The gravity core is 4.47 m long and contains coral fragments throughout, and its stratigraphy refers to a time span between 9 and 12 kyr BP (late Younger Dryas and early Holocene; Fink et al., 2013; Wang et al., 2021). For

this core, we used previously published data (Table 1) based on five accelerator mass spectrometry (AMS) radiocarbon ( $^{14}\text{C}$ ) coral ages, which were originally published by Fink et al. (2013), and 10 additional Th/U dates published by Wang et al. (2021).

The off-mound core GeoB13731-1 was collected from the adjacent seafloor within the EMCP on the continental slope in between the two on-mound cores (10 and 4 km distance, Fig. 1) during the R/V *Poseidon* cruise POS385. The gravity core is 4.31 m long and covers the last 23 kyr (Fink et al., 2013; Wang et al., 2021), including the mound formation phase covered by on-mound core GeoB13729-1, thus making it suitable for comparison. For this core, we use previously published data from Fink et al. (2013; seven AMS  $^{14}\text{C}$  ages; Table 1). From the same site, the off-mound core MD13-3457 was collected using a Calypso piston corer on board R/V *Marion Dufresne* during expedition MD194 (Van Rooij et al., 2013). With a core recovery of 20.31 m, it provides a stratigraphically longer record and was therefore dated and included in the analysis to extend our comparison between on- and off-mound records towards MIS5, i.e. the latest mound formation phase covered by on-mound core GeoB18116-2.

While the raw data measurements in this study were performed on the Dragon Mound core (GeoB18116-2) and the long off-mound core (MD13-3457), (raw) data from BRI (GeoB13729-1) and the shorter off-mound core (GeoB13731-1) have previously been published. The latter data have been obtained using the same protocols and were eventually processed for the specific purpose of this study. The detailed origin of all raw data is outlined for each methodological step and in Table 1.

### 3.1 Computed tomography of on-mound cores GeoB18116-2 and GeoB13729-1

Computed tomography (CT) scans were performed on on-mound core GeoB13729-1 (previously published in Titschack et al., 2016) and the coral-bearing part of the MeBo core GeoB18116-2 (the upper  $\sim 60$ – $61$  m, this study). The coral-bearing core sections of GeoB18116-2 were frozen at  $-20^\circ\text{C}$  and split length-wise with a stone saw into a “work” half for sediment sampling and an “archive” half (undisturbed) for CT scanning. The MeBo core was scanned at a resolution of 0.3 mm using a Philips Brilliance iCT Elite 256 computer tomograph with an X-ray source voltage of 120 kV and a current of 300 mA (Klinikum Bremen-Mitte, Germany). CT data were processed using the ZIB edition of Amira software, version 2022.31 (Stalling et al., 2005), closely following the approach of Titschack et al. (2015, 2016). Accordingly, the segmentation of the macrofossil fraction and the sediment was based on thresholding followed by watershedding, and all macrofossils  $>1$  mm within the sediment were quantified. The parameters given for each core depth at an 0.3 mm interval include the mean X-ray at-

tenuation in Hounsfield units (HU) and sediment and macrofossil contents in volume percent (vol %). Since the macrofossil content consists predominantly of corals, their fraction is referred to as the “coral content” in the following (sensu Titschack et al., 2016). The data points corresponding to the outlined parameters were averaged to a 5 cm resolution using a running average function. In the specific case of the MeBo core GeoB18116-2, each core barrel ( $n = 26$ ; each is  $\sim 235$  cm in length, including a core catcher) was treated individually. CT orthoslice images, 3D clast quantification, clast size, clast orientation and coral content, and mean X-ray attenuation and its standard deviation (SD) are presented for each core barrel, along with its corresponding depth, in the Supplement.

### 3.2 Depth model of MeBo core GeoB18116-2 (Dragon Mound)

For the purpose of this study, a new depth model was introduced that compensates for core expansion ( $>100\%$  recovery) in MeBo core GeoB18116-2, calculated according to the International Ocean Discovery Program (IODP) core depth below sea floor B (CSF-B; IODP depth scales terminology standards; IODP, 2011). This new depth model results in some minor depth differences compared to the depth model of Wienberg et al. (2022), which was calculated according to the IODP core depth below sea floor A (CSF-A) standard, and results in some minor differences in the calculated mound aggradation rates (ARs). While CSF-A refers to the drill top depth of the barrel and adds the length of core recovery (allowing core overlap by core recoveries exceeding 100 %), this study refers to CSF-B, which uses linear interpolation to recalculate, i.e. compress, the core recovery length to the core barrel length when it exceeds 100 % recovery (correcting for core overlaps). This is necessary to assign more accurate depths to the data points obtained from the CT scan. Gaps in the sediment record (void air spaces) were also subtracted from the record and not counted as depth (CSF-B). In addition, several section tops showed an unusually high coral content for the first  $\sim 5$  cm. This is an effect specific to MeBo drilling, where core barrels are retrieved separately from the drill hole. As this may cause core breccia, i.e. coral fragments, to fall into the drill hole in between drilling sections, the corresponding data are considered inaccurate and were subsequently removed from the depth record and assigned to “no data”. The depth models are made available in the PANGAEA open-data repository. In the following, all core depths for GeoB18116-2 refer to the CSF-B depth model.

### 3.3 Age models

For core GeoB18116-2 (Dragon Mound), all coral ages ( $n = 76$ ) and the mound formation phases and mound ARs derived are based on Th/U dating of the scleractinian CWC *Lophe-*

**Table 1.** Metadata of sediment cores used for this study, including coordinates, water depth in metres below sea level (m b.s.l.), and core recovery in metres below sea floor (m b.s.f.). The time period covered by the cores and a description of the origin of all data (CT is computed tomography; TIC/TOC indicate total inorganic and organic carbon) are provided. References are as follows: 1 – Wienberg et al. (2022), 2 – Fink et al. (2013), 3 – Wang et al. (2021), and 4 – Titschack et al. (2016).

Core	Location	Depth [m b.s.l.]	Recovery [m b.s.f.]	Age [kyr BP]	Dating	CT	TIC/TOC and density
GeoB18116-2 Dragon Mound	35°18.64' N, 02°34.93' E	236	70.85	100-390	1	This study	This study
GeoB13729-1 Brittlestar Ridge 1	35°26.07' N, 02°30.83' E	442	4.47	9–12	2, 3	4	3
GeoB13731-1 Off-mound	35°24.80' N, 02°33.22' E	362	4.31	0–23	2, 3	N/A	3
MD13-3457 Off-mound	35° 24.80' N, 02°33.22' E	345	20.31	0–126	This study	N/A	This study

*lia pertusa* and were previously published by Wienberg et al. (2022). Coral ages range from 390 to 103 kyr BP and were assigned to six mound formation phases (DM1 to DM6, for each phase an average AR is provided); see Wienberg et al. (2022) for more detail. The mound formation phases are separated by hiatuses, i.e. periods without any CWC mound formation, which span remarkably long time periods of 10–90 kyr (Wienberg et al., 2022). Notably, several coral ages between ~20 and 27 m in core depth are scattered across a large time span covering MIS7d–MIS9, which results in low ARs of  $<15 \text{ cm kyr}^{-1}$ . Accordingly, this low-aggradation period (DM4) was classified as a period of slow mound formation, i.e. scarce reef growth, following Frank et al. (2009). Due to the CT-based high-resolution imagery and based on sudden changes in coral content, coral fragment orientation, and matrix sediment density (see Supplement), the exact positions of mound formation phase boundaries were newly determined for this study, resulting in slightly adapted boundary depths and ARs compared to Wienberg et al. (2022). The depth of the mound base is slightly deeper than the deepest coral age obtained; consequently, the AR for DM1 during MIS11 is likely underestimated.

The age model of on-mound core GeoB13729-1 (Brittlestar Ridge I) is provided by Wang et al. (2021) and is partly based on coral ages from Fink et al. (2013, Table 1). The record documents one mound formation phase between 9 and 12 kyr BP, which is the last of several mound formation phases on BRI (Fentimen et al., 2020; Wienberg et al., 2022; Fentimen et al., 2022). This phase will hereafter be referred to as “BRI<sub>final</sub>”. Notably, BRI<sub>final</sub> has also been documented in several other cores collected from BRI (Fink et al., 2013; Stalder et al., 2018; Fentimen et al., 2020; Fentimen et al., 2022; Wienberg et al., 2022; Fentimen et al., 2023; Korpanty et al., 2023), showing that BRI<sub>final</sub> started earlier than documented in core GeoB13729-1. However, Wienberg et al. (2022), who investigated the entire phase covering

coral ages from 15 to 8 kyr BP, found overall ARs of 130–140  $\text{cm kyr}^{-1}$ , which match well with the AR for BRI<sub>final</sub> used in this study (135  $\text{cm kyr}^{-1}$ ; Wang et al., 2021), supporting the use of GeoB13729-1 for our purposes despite it not covering the entire mound formation phase.

The age model of off-mound core MD13-3457 was created for this study and is based on eight AMS  $^{14}\text{C}$  ages obtained from mixed-planktonic foraminifera. Measurements were performed on  $>15 \text{ mg}$  of planktonic foraminifera  $>150 \mu\text{m}$  at the Poznan Radiocarbon Laboratory, Poland. Additionally, the stable oxygen isotope ( $\delta^{18}\text{O}$ ) composition of the epi-benthic foraminifera *Cibicides mundulus* was analysed for ~10 specimens in the same size fraction at a 5 cm core resolution to extend the age model of core MD13-3457. Measurements were performed using a Finnigan MAT 252 gas isotope ratio mass spectrometer connected to a Kiel II automated carbonate preparation device at the MARUM, University of Bremen, Germany. For oxygen isotope analysis, a working standard was used (standard deviation =  $\pm 0.09 \text{‰}$   $\delta^{18}\text{O}$ ), calibrated against the NBS 19 standard and reported relative to the Vienna Pee Dee Belemnite standard. The age model of core GeoB13731-1 is based on seven  $^{14}\text{C}$  ages previously published by Fink et al. (2013) and Wang et al. (2021) but is revised for this study).

For both off-mound cores, age models were produced with the Undatable software (version 1.31; Loughheed and Obrochta, 2019) in Matlab (R2021b version 7) using  $10^5$  Monte Carlo iterations of age uncertainty sampling. AMS  $^{14}\text{C}$  ages from both off-mound cores were calibrated using the IntCal20 calibration curve (Reimer et al., 2020) and modelled reservoir ages from Butzin et al. (2017), extracted with Palaeo Data View (PDV) software (Langner and Mulitza, 2019). For core MD13-3457, additional tie points were set in PDV by comparing the global benthic LR04 stack (Lisiecki and Raymo, 2005) with our  $\delta^{18}\text{O}$  record. The age error of the tie points was conservatively set at 4 kyr, since this is the

estimated uncertainty of the benthic stack curve of Lisiecki and Raymo (2005) for 1 Myr until present.

Sedimentation rates were calculated using linear interpolation between calibrated ages (and tie points) for both cores (see Supplement for more detail). By working with a consistent methodology for both off-mound cores, we provide the first age model for core MD13-3457 and update the age model of core GeoB13731-1 (see Wang et al., 2021).

### 3.4 Matrix sediment dry-bulk-density measurements

Sediment samples of 6–10 cm<sup>3</sup> were taken from the on-mound core GeoB18116-2 and the off-mound core MD13-3457 to determine dry bulk densities (DBDs). DBD data from on-mound core GeoB13729-1 ( $n = 22$ ) and off-mound core GeoB13731-1 ( $n = 22$ ) were generated by Wang et al. (2021) following the same procedure as outlined below (data available at <https://doi.pangaea.de/10.1594/PANGAEA.941018>, Wang et al., 2025).

Samples from core GeoB18116-2 were collected at the approximate beginning and end of each mound formation phase ( $n = 18$ ; range: 1.17–1.40 g cm<sup>-3</sup>). The off-mound core MD13-3457 was sampled for DBD measurements at equal distances of 1 m ( $n = 21$ ; range: 0.88–1.44 g cm<sup>-3</sup>). The DBD measurements were performed following Ocean Drilling Program (ODP) standards (Blum, 1997). Samples were dried for 24 h at 105 °C, and their weight was measured before and after. Then, dry sediment volumes were determined using a PentaPyc 5200e gas pycnometer (Quantachrome Instruments) in the Geotechnical Laboratory at the MARUM, University of Bremen, Germany. Since GeoB18116-2 was scanned by CT, we then followed an additional approach for this core: as CT X-ray attenuation data have been used as a proxy for DBD in the past (Orsi et al., 1994; Gerland and Villinger, 1995; Orsi and Anderson, 1999; Duchesne et al., 2009) and as we have observed a high linear correlation ( $R^2 = 0.89$ ;  $p$ -val.  $\leq 0.0001$ ) between DBD and X-ray attenuation data throughout GeoB18116-2 (see Supplement for calibration details), we calculated DBD values from the X-ray attenuation data for core GeoB18116-2. This highly increased the resolution of our sediment density data and may be an alternative, non-invasive, and time-efficient methodology to obtain density data for similar purposes.

### 3.5 Total organic and inorganic carbon analysis

Sediment samples of 6–10 cm<sup>3</sup> were collected from on-mound core GeoB18116-2 and off-mound core MD13-3457 to measure the total organic carbon (TOC) and total inorganic carbon (TIC) content. TIC/TOC data from cores GeoB13729-1 ( $n = 44$ ) and GeoB13731-1 ( $n = 43$ ) were obtained by Wang et al. (2021) at 10 and 5 cm resolutions, respectively, following the same procedure as outlined below (data available at <https://doi.pangaea.de/10.1594/PANGAEA.941018>).

Samples from the on-mound core GeoB18116-2 ( $n = 54$ ) were collected at core levels corresponding to roughly comparable age intervals. Off-mound core MD13-3457 was sampled every 10 cm ( $n = 169$ ) from a core depth of 355 cm downwards to account for the record that is not already covered by the off-mound core GeoB13731-1. Macrofossil fragments of ca. >2 mm were removed from the sample to avoid misrepresentation of the sediment fraction, and then the freeze-dried samples were ground. From each sample, one subsample (~100 mg) was analysed for total carbon (TC) and one for TOC after it was treated with hydrochloric acid to remove carbonate. Measurements were performed with a LECO CS 744 at the Department of Geosciences, University of Bremen, Germany. Subsequently, the TIC content was calculated as  $TIC = TC - TOC$ , all given in weight percent (wt %).

### 3.6 Methods of calculating carbon(ate) accumulation

We calculated the total carbon accumulation, which consists of three different carbon fractions: (1) the coral inorganic carbon accumulation (coral  $C_{inorg}$  Acc), specific to the on-mound cores; (2) the sediment inorganic carbon accumulation (sediment  $C_{inorg}$  Acc); and (3) the sediment organic carbon accumulation (sediment  $C_{org}$  Acc).

#### 3.6.1 Coral inorganic carbon accumulation

Coral  $C_{inorg}$  Acc (g C cm<sup>-2</sup> kyr<sup>-1</sup>) for core GeoB18116-2 (Dragon Mound, 1138 data points spanning the upper 61.27 m (CSF-B)) and core GeoB13729-1 (43 data points, 0.05–4.25 m) was calculated closely following the methodology outlined in Titschack et al. (2015, 2016). Thus, a coral density of 2.66 g cm<sup>-3</sup> (i.e. 100 % carbonate; Dorschel et al., 2007b) was multiplied by the coral content (vol %) from the CT data. Combined with the corresponding mound ARs [cm kyr<sup>-1</sup>], coral carbonate accumulation [g CaCO<sub>3</sub> cm<sup>-2</sup> kyr<sup>-1</sup>] was first determined for each 5 cm average depth point.

Coral  $C_{inorg}$  Acc =

$$\text{Coral vol. \%} \times \text{Coral density} \times \text{AR} \times \frac{12.01}{100.09} \quad (1)$$

Accounting for the molecular weight fraction of carbon within carbonate (i.e. 12 % C in CaCO<sub>3</sub>, ratio in g mol<sup>-1</sup>; see Eq. 1), coral carbonate accumulation was then converted to coral  $C_{inorg}$  Acc.

#### 3.6.2 Sediment organic and inorganic carbon accumulation

Sediment  $C_{inorg}$  Acc and sediment  $C_{org}$  Acc (g C cm<sup>-2</sup> kyr<sup>-1</sup>) were determined using the following

equation:

$$\text{Sed. } C_{(\text{in})\text{org}} \text{ Acc} = C_{(\text{in})\text{org}} \text{ wt} \% \times \text{Sed. vol.} \% \times \text{Sed. density} \times \text{AR.} \quad (2)$$

The sediment  $C_{\text{org}}$  and  $C_{\text{inorg}}$  contents (Sect. 3.5) were multiplied by the CT-derived matrix sediment volume percent (Sect. 3.1; in the case of the coral-bearing on-mound cores since only part of the total volume consists of matrix sediment). Then, each data point was assigned a matrix sediment DBD value ( $\text{g cm}^{-3}$  based on linear interpolation or, if available, CT calibration; Sect. 3.4) at the given depth and multiplied. Each of the core depths with  $C_{\text{org}}$  and  $C_{\text{inorg}}$  values [ $\text{g cm}^{-3}$ ] was then assigned to a corresponding AR and multiplied again. Eventually, this results in a sediment  $C_{\text{inorg}}$  and  $C_{\text{org}} \text{ Acc}$  [ $\text{g C cm}^{-2} \text{ kyr}^{-1}$ ]; see Eq. (2). This was calculated for both CWC-bearing cores and both off-mound records for comparison. Sediment  $C_{\text{inorg}}$  [ $\text{g cm}^{-3}$ ] may also be converted to carbonate using the molecular weight share described above in order to describe the total carbonate accumulation (coral carbonate and sediment carbonate).

### 3.6.3 Total carbon accumulation

To determine the total carbon accumulation (Eq. 3) for the CWC mounds studied, the CT-based coral  $C_{\text{inorg}} \text{ Acc}$  data points were downscaled to the resolution of the  $C_{\text{org}}$  and  $C_{\text{inorg}}$  data (i.e. 54 data points for core GeoB18116-2 and 44 data points for core GeoB13729-1 from the TIC/TOC measurements). Then, all data points within a mound formation phase were averaged, and mean, minimum, and maximum values per mound formation phase are provided for total carbon accumulation, coral  $C_{\text{inorg}} \text{ Acc}$ , sediment  $C_{\text{inorg}} \text{ Acc}$ , and sediment  $C_{\text{org}} \text{ Acc}$ . Additionally, we present the same for carbonate accumulation (total carbonate accumulation, i.e. coral carbonate and sediment carbonate accumulation). Ultimately, we obtain the relative contribution (%) of each carbon fraction to the total carbonate and total carbon accumulation.

$$C_{\text{total}} \text{ Acc} = \text{Coral } C_{\text{inorg}} \text{ Acc} + \text{Sed. } C_{\text{inorg}} \text{ Acc} + \text{Sed. } C_{\text{org}} \text{ Acc} \quad (3)$$

The total carbon accumulation ( $\text{g C cm}^{-2} \text{ kyr}^{-1}$ ) was also obtained for both off-mound cores (sediment  $C_{\text{inorg}} \text{ Acc}$  and sediment  $C_{\text{org}} \text{ Acc}$ ). Here, we use weighted-mean values of accumulation rates from the off-mound core corresponding to a specific mound formation phase in the on-mound cores. This facilitates a comparison of mean carbon accumulation between on- and off-mound settings during the same time interval (Table 1). While samples from core GeoB13731-1 (9–12 kyr BP;  $n = 6$ ) were used to compare the carbon accumulation rates with the latest mound formation phase ( $\text{BRI}_{\text{final}}$ ) (GeoB13729-1;  $n = 43$ ), core MD13-3457 (108–115 kyr BP;  $n = 10$ ) was used to compare with the latest mound formation phase (DM6) preserved in Dragon Mound (GeoB18116-

2;  $n = 9$ ). All parameters from the off-mound cores were averaged and compared with regard to that exact time span, rounded up to the kyr scale.

## 4 Results

### 4.1 On-mound carbon(ate) accumulation

#### 4.1.1 Dragon Mound record: results from a 61 m long CT scan

A visual inspection of the CT scans revealed that the coral content of core GeoB18116-2 was mainly composed of *Lophelia pertusa*, with minor contributions of dendrophylliid corals. The average coral content is 14 vol % (5 cm average), with a maximum of 42 vol % (for core sections with high coral content, see Fig. 2a). There are no major coral-barren units and some clearly visible hiatuses (Fig. 2b). The mound base lies at  $\sim 61.1$  m b.s.f. (CSF-B depth; Fig. 2c).

Based on the CT-derived localisation of mound formation phase boundaries and considering the new core depth model (CSF-B), the newly calculated ARs of the individual mound formation phases deviate slightly from those previously published by Wienberg et al. (2022; see Table 2). The mound initiation phase, DM1 ( $\sim$  MIS11), shows an AR of  $22 \text{ cm kyr}^{-1}$ , followed by DM2 and DM3 ( $\sim$  MIS9b-d and MIS10), corresponding to an AR of  $61 \text{ cm kyr}^{-1}$  each. The slow mound formation phase, DM4 ( $\sim$  MIS7d–MIS9), has an AR of  $11 \text{ cm kyr}^{-1}$ ; during DM5 ( $\sim$  MIS7b), ARs amount to  $131 \text{ cm kyr}^{-1}$ , and the most recent mound formation phase, DM6 ( $\sim$  MIS5d), has the highest AR, with  $147 \text{ cm kyr}^{-1}$  (Fig. 3; Table 2).

For further details on all raw core data results (DBD, TIC/TOC, and CT coral volumes; CT raw data; and the off-mound AMS  $^{14}\text{C}$  ages obtained) that fed into the calculation of carbon accumulation rates, please refer to the Supplement and PANGAEA open-data repository.

#### 4.1.2 Carbonate accumulation rates

Total mean on-mound carbonate accumulation rates averaged across each defined mound formation phase from the sediment cores collected from Dragon Mound and BRI lie between  $49$  and  $115 \text{ g CaCO}_3 \text{ cm}^{-2} \text{ kyr}^{-1}$  for DM2, DM3, DM5, DM6, and  $\text{BRI}_{\text{final}}$  (Fig. 3, Table 2). Exhibiting mean rates of  $105$ – $115 \text{ g CaCO}_3 \text{ cm}^{-2} \text{ kyr}^{-1}$  (range:  $71$ – $167 \text{ g CaCO}_3 \text{ cm}^{-2} \text{ kyr}^{-1}$ ), the youngest “enhanced” mound formation phases (DM5, DM6, and  $\text{BRI}_{\text{final}}$ ) are all in the same range and are more than twice as high as the rates from the earlier mound formation phases (DM2 and DM3), which show mean rates of  $49$  and  $53 \text{ g CaCO}_3 \text{ cm}^{-2} \text{ kyr}^{-1}$  (range:  $32$ – $66 \text{ g CaCO}_3 \text{ cm}^{-2} \text{ kyr}^{-1}$ ). The mound initiation phase, DM1, as well as the slow mound formation phase, DM4, show much lower rates, with  $16$  and  $11 \text{ g CaCO}_3 \text{ cm}^{-2} \text{ kyr}^{-1}$  (range:  $9$ – $19 \text{ g CaCO}_3 \text{ cm}^{-2} \text{ kyr}^{-1}$ ),

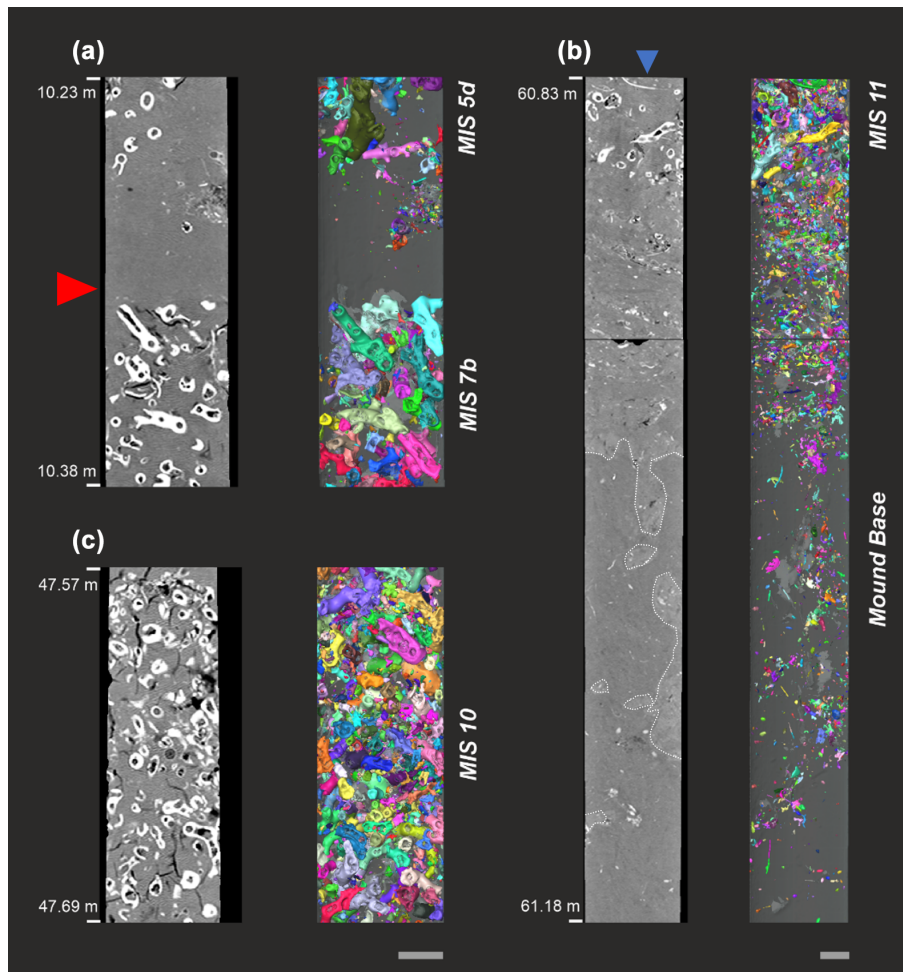


**Figure 2.** CT-image-based core section close-ups of the MeBo on-mound core GeoB18116-2 collected from Dragon Mound (left is the orthoslice; right is the 3D macrofossils' reconstruction: each coral fragment has an individual colour and the core depth is given in CSF-B metres below seafloor). **(a)** Hiatus covering a time span of  $\sim 100$  kyr between mound formation phases DM5 and DM6. The red arrow indicates the top of DM5 (coral ages  $\sim$  MIS7b), followed by DM6 (coral ages  $\sim$  MIS5d). **(b)** Example of a high-coral-carbonate-bearing unit during the mound formation phase, DM2 (MIS10,  $\sim 350$  kyr BP). **(c)** Scan of the mound base (61.1 m b.s.f.), including burrows filled with cold-water coral mound sediments (white outlines), the first cold-water coral clasts, and several oyster shells (blue arrow) from DM1 ( $\sim$  MIS11). Grey scale bars at the bottom represent  $\sim 2$  cm in length.

respectively. Overall, the contribution of the coral carbonate fraction to the total mound carbonate accumulation (Fig. 3, Table 2) varies between 32 %–56 % (DM1 and BRI<sub>final</sub>, respectively) throughout the mound formation phases. Accordingly, the carbonate derived from the sediment matrix (sediment carbonate) contributes 44 %–68 % to the total mound carbonate accumulation.

#### 4.1.3 Carbon accumulation rates

Total mean mound carbon accumulation rates averaged across the defined mound formation phases amount to  $6\text{--}15\text{ g C cm}^{-2}\text{ kyr}^{-1}$  for DM2, DM3, DM5, DM6, and BRI<sub>final</sub> (range:  $4\text{--}21\text{ g C cm}^{-2}\text{ kyr}^{-1}$ ; Fig. 3, Table 3). Analogous to the carbonate accumulation, the three most

recent mound formation phases show a comparable total carbon accumulation rate of  $14\text{--}15\text{ g C cm}^{-2}\text{ kyr}^{-1}$  (range:  $10\text{--}21\text{ g C cm}^{-2}\text{ kyr}^{-1}$ ), while during DM2 and DM3, accumulation was  $\sim 50$  % lower (mean of 6 and  $7\text{ g C cm}^{-2}\text{ kyr}^{-1}$ , respectively; range:  $4\text{--}8\text{ g C cm}^{-2}\text{ kyr}^{-1}$ ). During the slow mound formation phase (DM4) and the Dragon Mound initiation phase (DM1), only  $1.3\text{--}2.1\text{ g C cm}^{-2}\text{ kyr}^{-1}$  (range:  $1.1\text{--}2.4\text{ g C cm}^{-2}\text{ kyr}^{-1}$ ) accumulated.

The  $C_{\text{inorg}}$  Acc accounts for the largest contribution to total carbon accumulation here, with coral  $C_{\text{inorg}}$  varying between 30 %–52 % and sedimentary  $C_{\text{inorg}}$  between 41 %–63 %. The sedimentary  $C_{\text{org}}$  fraction contributes  $0.1\text{--}1.3\text{ g C cm}^{-2}\text{ kyr}^{-1}$  (range:  $0.1\text{--}1.5\text{ g C cm}^{-2}\text{ kyr}^{-1}$ ), which is 6 %–9 % of the total mound accumulation amongst the

**Table 2.** All rates of mound aggradation (AR), carbonate accumulation (Acc), and fraction contribution (%) per mound formation phase (Brittlestar Ridge I is BRI<sub>final</sub>; Dragon Mound is DM6–DM1) for coral- and sediment-derived carbonate. The minimum–maximum range is given in brackets. The “age” column indicates the duration of the mound formation phase based on coral ages. The “period” column indicates the approximate corresponding marine isotope stage (MIS). Carbonate-related mean values are given in bold; core locations are in italics.

Mound formation phases	Age [kyr BP]	Period [MIS]	AR [cm kyr <sup>-1</sup> ]	Total carbonate Acc [g CaCO <sub>3</sub> cm <sup>-2</sup> kyr <sup>-1</sup> ]	Coral carbonate Acc [g CaCO <sub>3</sub> cm <sup>-2</sup> kyr <sup>-1</sup> ]	%	Sediment carbonate Acc [g CaCO <sub>3</sub> cm <sup>-2</sup> kyr <sup>-1</sup> ]	%
<i>Brittlestar Ridge I (GeoB13729-1)</i>								
BRI <sub>final</sub>	9–12	MIS1	135	<b>110</b> (71–167)	<b>61.5</b> (21–127)	56	<b>48.1</b> (39–57)	44
<i>Dragon Mound (GeoB18116-2)</i>								
DM6	108–115	MIS5d	147	<b>105</b> (86–144)	<b>34.6</b> (12–73)	33	<b>70.6</b> (68–73)	67
DM5	201–208	MIS7b	131	<b>115</b> (87–142)	<b>52.8</b> (14–86)	46	<b>62.0</b> (52–73)	54
DM4	220–285	MIS7d–9	11	<b>11</b> (9–12)	<b>5.3</b> (4–7)	50	<b>5.3</b> (4–6)	50
DM3	297–319	MIS9b–d	61	<b>49</b> (38–56)	<b>18.0</b> (2–26)	37	<b>31.0</b> (28–36)	63
DM2	340–367	MIS10	61	<b>53</b> (32–66)	<b>21.0</b> (2–37)	40	<b>31.7</b> (25–38)	60
DM1	372–390	MIS11	22	<b>16</b> (15–19)	<b>5.2</b> (3–8)	32	<b>11.1</b> (10–12)	68

**Table 3.** All rates of mound aggradation (AR), mound carbon accumulation (Acc), and contribution (%) per mound formation phase (Brittlestar Ridge I is BRI<sub>final</sub>; Dragon Mound is DM6–DM1) for coral- and sediment-derived inorganic carbon (coral C<sub>inorg</sub>, sediment C<sub>inorg</sub>), in addition to the organic carbon fraction from the mound sediment (sediment C<sub>org</sub>) relative to the total carbon accumulation. The minimum–maximum range is given in brackets. The “age” column indicates the duration of the mound formation phase based on coral ages. The “period” column indicates the approximate corresponding marine isotope stage (MIS). Carbonate-related mean values are given in bold; core locations are in italics.

Mound formation phases	Age [kyr BP]	Period [MIS]	AR [cm kyr <sup>-1</sup> ]	Total carbon Acc [g C cm <sup>-2</sup> kyr <sup>-1</sup> ]	Coral C <sub>inorg</sub> Acc [g C cm <sup>-2</sup> kyr <sup>-1</sup> ]	%	Sediment C <sub>inorg</sub> Acc [g C cm <sup>-2</sup> kyr <sup>-1</sup> ]	%	Sediment C <sub>org</sub> Acc [g C cm <sup>-2</sup> kyr <sup>-1</sup> ]	%
<i>Brittlestar Ridge I (GeoB13729-1)</i>										
BRI <sub>final</sub>	9–12	MIS1	135	<b>14.1</b> (10–21)	<b>7.38</b> (2.5–15.2)	52	<b>5.77</b> (4.7–6.9)	41	<b>0.99</b> (0.6–1.2)	7
<i>Dragon Mound (GeoB18116-2)</i>										
DM6	108–115	MIS5d	147	<b>13.9</b> (12–18)	<b>4.15</b> (1.5–8.8)	30	<b>8.47</b> (8.2–8.8)	61	<b>1.26</b> (0.9–1.5)	9
DM5	201–208	MIS7b	131	<b>14.7</b> (12–18)	<b>6.33</b> (1.6–10.4)	43	<b>7.44</b> (6.2–8.8)	51	<b>0.96</b> (0.7–1.2)	6
DM4	220–285	MIS7d–9	11	<b>1.3</b> (1.1–1.6)	<b>0.63</b> (0.4–0.8)	47	<b>0.63</b> (0.5–0.7)	47	<b>0.08</b> (0.06–0.10)	6
DM3	297–319	MIS9b–d	61	<b>6.4</b> (5.1–7.1)	<b>2.16</b> (0.3–3.2)	34	<b>3.72</b> (3.3–4.3)	58	<b>0.55</b> (0.4–0.7)	8
DM2	340–367	MIS10	61	<b>6.7</b> (4.2–8.3)	<b>2.52</b> (0.2–4.4)	37	<b>3.81</b> (3.0–4.6)	57	<b>0.40</b> (0.3–0.5)	6
DM1	372–390	MIS11	22	<b>2.1</b> (2.0–2.4)	<b>0.63</b> (0.3–1.0)	30	<b>1.33</b> (1.2–1.5)	63	<b>0.16</b> (0.1–0.2)	7

studied sites. For all carbon fractions individually, DM5, DM6, and BRI<sub>final</sub> exhibit the highest accumulation values, a factor of  $\sim 2$  higher than during DM2 and DM3, which in turn exceed DM1 and DM4 by a factor of  $\sim 2$  (Fig. 3, Table 3).

#### 4.2 Off-mound carbon(ate) accumulation rates

The two combined off-mound cores cover a time span of 0–126 kyr BP. During BRI<sub>final</sub>, the off-mound record GeoB13731-1 accounts for a mean sedimentation rate (SR) of 16 cm kyr<sup>-1</sup> and a total mean carbonate accumulation of 7.25 g CaCO<sub>3</sub> cm<sup>-2</sup> kyr<sup>-1</sup> (range: 4.17–9.83 g CaCO<sub>3</sub> cm<sup>-2</sup> kyr<sup>-1</sup>; based on data from Wang et al., 2021). The total mean carbon accumulation accounts for 0.99 g C cm<sup>-2</sup> kyr<sup>-1</sup> (range: 0.56–1.33 g C cm<sup>-2</sup> kyr<sup>-1</sup>), comprising a sediment C<sub>org</sub> Acc of 0.11 g C cm<sup>-2</sup> kyr<sup>-1</sup>

(range: 0.05–0.16 g C cm<sup>-2</sup> kyr<sup>-1</sup>) and a sediment C<sub>inorg</sub> Acc of 0.87 g C cm<sup>-2</sup> kyr<sup>-1</sup> (range: 0.50–1.18 g C cm<sup>-2</sup> kyr<sup>-1</sup>; based on data from Wang et al., 2021).

During DM6, the off-mound record MD13-3457 accounts for a mean sedimentation rate of 12 cm kyr<sup>-1</sup> and a mean carbonate accumulation rate of 5.50 g CaCO<sub>3</sub> cm<sup>-2</sup> kyr<sup>-1</sup> (range: 3.83–7.25 g CaCO<sub>3</sub> cm<sup>-2</sup> kyr<sup>-1</sup>). The total mean carbon accumulation accounts for 0.75 g C cm<sup>-2</sup> kyr<sup>-1</sup> (range: 0.52–0.98 g C cm<sup>-2</sup> kyr<sup>-1</sup>) comprising sediment C<sub>org</sub> Acc of 0.09 g C cm<sup>-2</sup> kyr<sup>-1</sup> (range: 0.06–0.12 g C cm<sup>-2</sup> kyr<sup>-1</sup>) and sediment C<sub>inorg</sub> Acc of 0.66 g C cm<sup>-2</sup> kyr<sup>-1</sup> (range: 0.46–0.87 g C cm<sup>-2</sup> kyr<sup>-1</sup>).

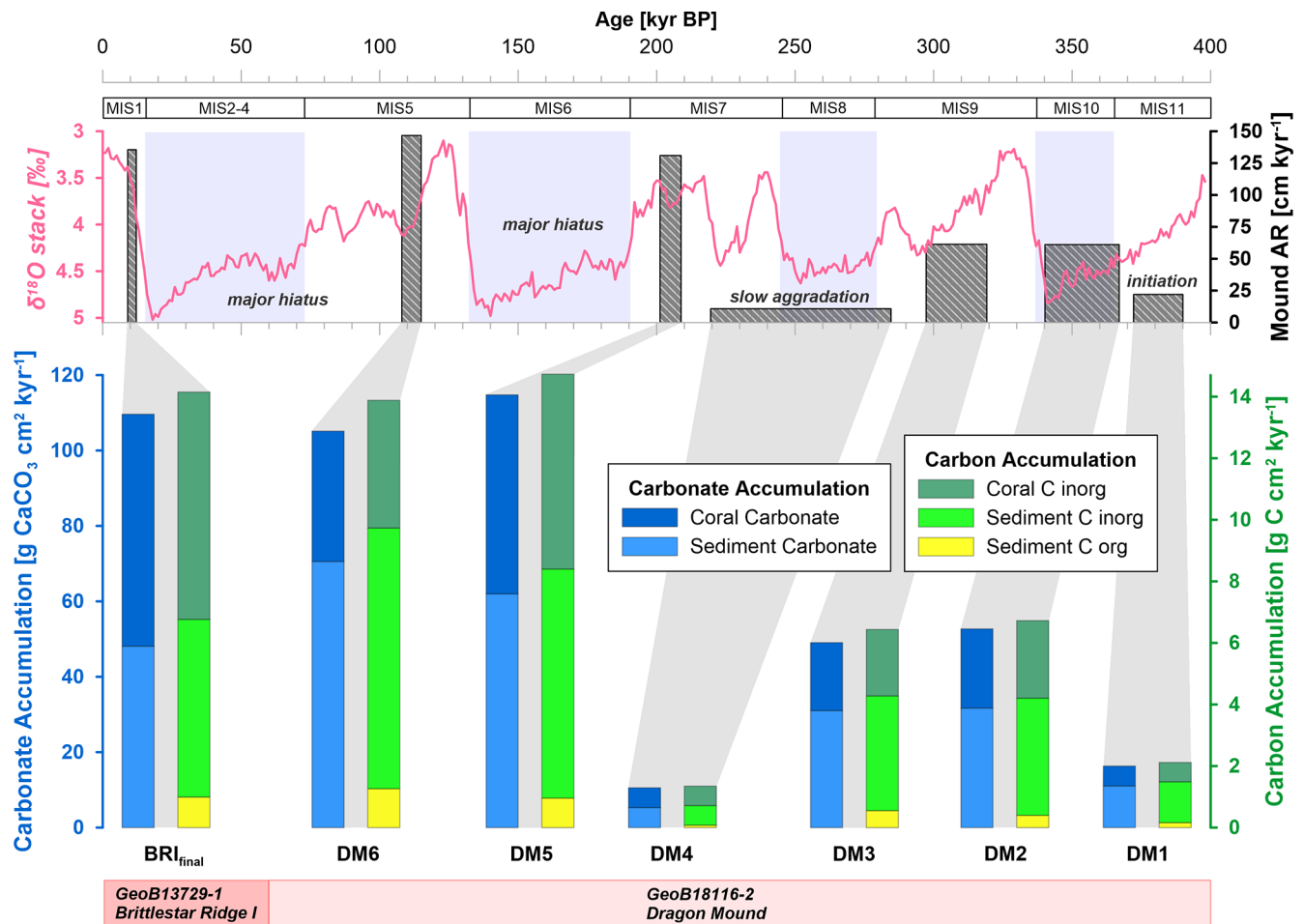


**Figure 3.** Illustration of the carbonate accumulation (blue colours) and carbon accumulation (green–yellow colours) for Dragon Mound and Brittlestar Ridge I (BRI) based on each mound formation phase (Brittlestar Ridge I is BRI<sub>final</sub>; Dragon Mound is DM6–DM1). Mound formation phases (duration to scale) and aggradation rate (AR) are shown in the top graph. The top  $x$  axis provides a timescale and corresponding global climate variations according to the benthic  $\delta^{18}\text{O}$  stack (pink curve) by Lisiecki and Raymo (2005), with marine isotope stages (MISs) indicated above. Glacial periods are highlighted by light-blue bars. The bottom graph shows the contribution of each carbon(ate) fraction to the total. Note that the bar width for the lower graph has no timescale, and carbonate and carbon accumulation rates are scaled to different axes (left and right  $y$  axes, respectively).

### 4.3 On-mound versus off-mound carbon accumulation rates

The comparison of synchronously deposited off-mound (GeoB13731-1 and MD13-3457) and the on-mound core sequences (GeoB13729-1 and GeoB18116-2) for the last two periods of mound formation reveals contrasting carbon contents and accumulation rates (Fig. 4, Table 4).

During the mound formation phase, BRI<sub>final</sub>, the sediment  $\text{C}_{\text{org}}$  content (wt %) is about 1.4 times higher on the CWC mound compared to the off-mound record (Fig. 4, Table 4). During the mound formation phase, DM6, the sediment  $\text{C}_{\text{org}}$  content is about 1.2 times higher on the mound. The mean sediment  $\text{C}_{\text{inorg}}$  content is just slightly higher on the CWC mounds compared to the off-mound records (a ratio of 1.1

for both periods). Thus, all mean carbon content values (sediment  $\text{C}_{\text{org}}$  and sediment  $\text{C}_{\text{inorg}}$ ) are higher on the mounds.

The difference between on- and off-mound records becomes clearer when comparing the accumulation rates during the same time period (Fig. 4, Table 4). Most importantly, all carbon accumulation rates during BRI<sub>final</sub> and DM6 are around an order of magnitude higher compared to those of the off-mound cores GeoB13731-1 and MD13-3457. During the mound formation phases BRI<sub>final</sub> and DM6, the sediment  $\text{C}_{\text{org}}$  Acc is 9 and 14 times higher on the CWC mounds than in the off-mound records, respectively. The sediment  $\text{C}_{\text{inorg}}$  Acc on the mounds exceeds the off-mound records by factors of 7 (BRI<sub>final</sub>) and 13 (DM6).

These factors increase to 15 (BRI<sub>final</sub>) and 19 (DM6) when also accounting for the coral  $\text{C}_{\text{inorg}}$  Acc in the on-mound records due to the lack of coral macrofossils in the off-mound

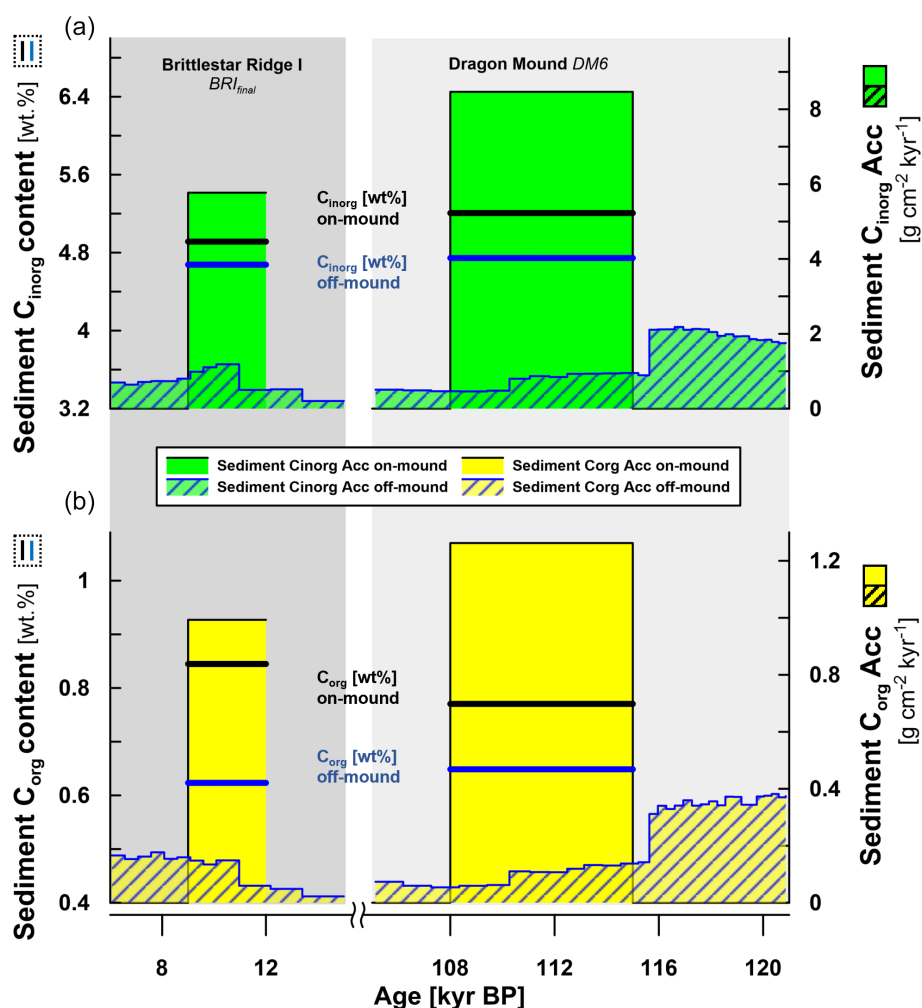


**Figure 4.** Comparison of sediment  $C_{\text{inorg}}$  and  $C_{\text{org}}$  contents (the bold lines show wt%; left y axes) and accumulation (Acc) rates (the filled bars show  $\text{g C cm}^{-2} \text{ kyr}^{-1}$ ; right y axes) between on- and off-mound cores, focusing on two mound formation phases (for the time span, see the x axis), with  $\text{BRI}_{\text{final}}$  on Brittlestar Ridge I corresponding to MIS1 (background highlighted in dark grey; GeoB13729-1 and GeoB13731-1) and DM6 on Dragon Mound corresponding to MIS5 (background highlighted in light grey; GeoB18116-2 and MD13-3457). (a) All  $C_{\text{inorg}}$  data are shown in the top half (green). (b) All  $C_{\text{org}}$  data are shown in the bottom half (yellow). All off-mound data have a blue outline; all on-mound data have a black outline. Carbon accumulation rates are shown as bars; carbon contents are shown as lines. Rates of on-mound records are shown as the mean per mound formation phase. Rates of off-mound records are shown at the TIC/TOC sample resolution, including the trend prior to and after the corresponding mound formation phase. For comparison, the mean  $C_{\text{org}}$  and  $C_{\text{inorg}}$  contents are displayed too. Note the x-axis break (15–105 kyr BP) between mound formation phases.

setting. The total carbon accumulation (coral  $C_{\text{inorg}}$ , sediment  $C_{\text{inorg}}$ , and sediment  $C_{\text{org}}$  Acc) on the mounds is 15 ( $\text{BRI}_{\text{final}}$ ) and 19 (DM6) times higher (Fig. 4, Table 4) compared to the off-mound environment during the same period, e.g. 9–12 and 108–115 kyr BP.

The data presented in Fig. 4 show contrasting trends for off-mound sediment  $C_{\text{org}}$  Acc between the mound formation phases. During and after  $\text{BRI}_{\text{final}}$ , off-mound  $C_{\text{org}}$  Acc increases, while before and throughout DM6, values decrease. At the same time,  $C_{\text{inorg}}$  Acc during  $\text{BRI}_{\text{final}}$  first increases in the off-mound record but then shows a sudden drop that continues after mound formation has ceased. During DM6,

$C_{\text{inorg}}$  Acc drops to a lower level. Generally, mean  $C_{\text{org}}$  and  $C_{\text{inorg}}$  contents in the off-mound cores are on the same level irrespective of the mound formation phase. Regarding the on-mound cores, mean  $C_{\text{org}}$  content is slightly higher on BRI than on Dragon Mound, while  $C_{\text{inorg}}$  content is slightly higher on Dragon Mound. At a glance, all mean carbon content and Acc values are higher for the CWC mounds despite large variations in the off-mound cores.

**Table 4.** All core data from the mound formation phases,  $BRI_{\text{final}}$  (documented in core GeoB13729-1, Brittlestar Ridge I (BRI)) and DM6 (documented in core GeoB18116-2, Dragon Mound) compared to the corresponding time interval measured in the off-mound cores GeoB13731-1 and MD13-3457, respectively. Columns show mound aggradation or sedimentation rate (AR or SR), organic carbon content ( $C_{\text{org}}$ ), inorganic carbon ( $C_{\text{inorg}}$ ) content, and carbon accumulation ( $C_{\text{org}}$  and  $C_{\text{inorg}}$  Acc). Total  $C_{\text{inorg}}$  Acc is composed of sediment  $C_{\text{inorg}}$  and coral  $C_{\text{inorg}}$ . The ratio indicates the factor by which the CWC mound exceeds the off-mound record (i.e. on mound : off mound). Available  $C_{\text{org}}$  and  $C_{\text{inorg}}$  content raw data points per mound formation phase are as follows: 43 (GeoB13729-1), 6 (GeoB13731-1), 9 (GeoB18116-2), and 10 (MD13-3457). The standard deviation is in brackets ( $\pm$ ). Carbon-related mean values are given in bold.

	AR or SR [cm kyr <sup>-1</sup> ]	$C_{\text{org}}$ [wt %]		$C_{\text{inorg}}$ [wt %]		Total carbon Acc [g C cm <sup>-2</sup> kyr <sup>-1</sup> ]		$C_{\text{inorg}}$ Acc [g C cm <sup>-2</sup> kyr <sup>-1</sup> ]		$C_{\text{org}}$ Acc [g C cm <sup>-2</sup> kyr <sup>-1</sup> ]			
								Sediment	Total				
9–12 kyr BP													
BRI	135	<b>0.84</b>	(0.07)	<b>4.91</b>	(0.39)	<b>14.1</b>	(2.9)	<b>5.77</b>	(0.48)	<b>13.16</b>	(2.99)	<b>0.99</b>	(0.14)
Off-mound	16	<b>0.62</b>	(0.12)	<b>4.68</b>	(0.34)	<b>1.0</b>	(0.3)	<b>0.87</b>	(0.29)	<b>0.87</b>	(0.29)	<b>0.11</b>	(0.05)
Ratio	8.5	<i>1.4</i>		<i>1.1</i>		<i>14.3</i>		<i>6.6</i>		<i>15.1</i>		<i>8.7</i>	
108–115 kyr BP													
DM6	147	<b>0.77</b>	(0.07)	<b>5.21</b>	(0.28)	<b>13.9</b>	(2.1)	<b>8.47</b>	(0.22)	<b>12.62</b>	(2.32)	<b>1.26</b>	(0.18)
Off-mound	12	<b>0.65</b>	(0.11)	<b>4.75</b>	(0.55)	<b>0.8</b>	(0.2)	<b>0.66</b>	(0.16)	<b>0.66</b>	(0.16)	<b>0.09</b>	(0.02)
Ratio	<i>12.6</i>	<i>1.2</i>		<i>1.1</i>		<i>18.5</i>		<i>12.8</i>		<i>19.1</i>		<i>14.0</i>	

## 5 Discussion

CWC mounds have been widely described as major carbonate factories (e.g. Titschack et al., 2009, 2015, 2016; Reijmer, 2021) with elevated carbonate accumulation rates and have been suggested to be potentially important local to regional carbonate sinks. Previous accumulation studies and broader estimates investigating CWC mounds off Norway, Ireland, Morocco, and Namibia and in the Mediterranean Sea found carbonate accumulation rates 2–11 times higher on the mounds compared to on the adjacent seafloor or the regional average (Lindberg and Mienert, 2005; Dorschel et al., 2007b; Titschack et al., 2009, 2015, 2016; Hebbeln et al., 2019; Tamborrino et al., 2022). However, just two studies have directly measured and compared carbonate accumulation on a mound to the immediate surrounding environment (Titschack et al., 2009, 2015), and all studies so far have focused on carbonate accumulation. This study provides a first holistic approach looking at the total carbon accumulation, including both  $C_{\text{inorg}}$  and  $C_{\text{org}}$  Acc on two mounds and two nearby off-mound records. To come to a conclusion about carbon accumulation rates and whether the CWC mounds studied are effective carbon sinks, comparability is essential. Ultimately, this raises the unresolved question of what time frames we should be looking at when discussing carbon sinks (Rossi and Rizzo, 2020).

The comparability of aggradation rates and, subsequently, carbon accumulation rates between different ecosystems (also different CWC mound records) depends strongly on the time interval considered. The time-averaging effect complicates comparisons between records, with generally decreasing aggradation rates corresponding to increasing time intervals analysed (e.g. Schlager, 2003). For instance, present-day

shallow-water coral reefs are carbonate factories that swing between states of active formation and extinction, being locally absent or displaced due to periodic sea level fluctuations and associated environmental change (e.g. Schlager, 1981; Milliman, 1993; Camoin and Webster, 2015; Wood et al., 2023). If carbon accumulation rates of such ecosystems are not only calculated for their active formation phase but also include periods of their temporal, local extinction, the time-averaging effects shift the accumulation rates to lower values. This also relates to rates within formation phases if the accumulation rates show large variations, as is the case in CWC mound records. Hence, any comparison of (CWC mound) carbonate and carbon accumulation rates has to be done with utter caution, with an awareness of whether these rates are calculated for large timescales across several (CWC mound) formation phases interrupted by periods of extinction (e.g. Titschack et al., 2009; the latter partly covering time intervals of hundreds of thousands of years), for intermediate timescales treating each (CWC mound) formation phase separately ( $\sim$  tens of thousands of years; this study), or for individual “units” within one (CWC mound) formation phase ( $\sim$  hundreds of years; e.g. Titschack et al., 2015). For instance, Norwegian CWC mound formation exhibits short-term maxima of up to  $>2000$  g  $\text{CaCO}_3$   $\text{cm}^{-2}$   $\text{kyr}^{-1}$  (Titschack et al., 2015). However, averaged across the entire mound formation phase record, aggradation and accumulation rates off Norway are on the same level as the enhanced mound formation phases described here ( $\sim 100$  g  $\text{CaCO}_3$   $\text{cm}^{-2}$   $\text{kyr}^{-1}$ ).

Thus, for consistency, we have chosen to look at complete mound formation phases, which are compared to the exact same period in the off-mound records. This approach allows the comparison of the mound formation phases dis-

cussed in this study with total mean rates from Titschack et al. (2015, 2016), who calculated accumulation rates over similar time spans ( $\sim 3$ – $8$  kyr). Ultimately, only studies that analysed core records covering similar time periods of at least 1 kyr were selected for further comparisons between CWC mound records or with other ecosystems.

### 5.1 Patterns of carbon(ate) accumulation in CWC mounds across space and time

Based on the mean and minimum–maximum range in total carbon(ate) accumulation for each mound formation phase in our study (Table 3), we identified three different groups of accumulation: phases of high carbon(ate) accumulation (DM5, DM6,  $BRI_{\text{final}}$ ; mean  $>100$  g  $\text{CaCO}_3$   $\text{cm}^{-2}$   $\text{kyr}^{-1}$  and  $\sim 15$  g  $\text{C cm}^{-2}$   $\text{kyr}^{-1}$ ), phases of moderate carbon(ate) accumulation (DM2, DM3;  $49$ – $53$  g  $\text{CaCO}_3$   $\text{cm}^{-2}$   $\text{kyr}^{-1}$  and  $6$ – $7$  g  $\text{C cm}^{-2}$   $\text{kyr}^{-1}$ ), and phases of slow carbon(ate) accumulation (DM1, DM4;  $<16$  g  $\text{CaCO}_3$   $\text{cm}^{-2}$   $\text{kyr}^{-1}$  and  $1$ – $2$  g  $\text{C cm}^{-2}$   $\text{kyr}^{-1}$ ). These correspond to high ( $>100$   $\text{cm kyr}^{-1}$ ), moderate ( $<100$  and  $>20$   $\text{cm kyr}^{-1}$ ), and low ( $<20$   $\text{cm kyr}^{-1}$ ) CWC mound ARs. A similar pattern has also been found for CWC mounds studied by Titschack et al. (2015, 2016) in Norway and the Mediterranean. For instance, compared to the high-carbonate-accumulating mound formation phases in this study ( $AR \sim 140$   $\text{cm kyr}^{-1}$ ;  $\sim 110$  g  $\text{CaCO}_3$   $\text{cm}^{-2}$   $\text{kyr}^{-1}$ ), the Norwegian CWC mounds of Træna Reef have very similar ARs ( $138$   $\text{cm kyr}^{-1}$ ) and accumulate a similar amount of carbonate, with  $103$  g  $\text{CaCO}_3$   $\text{cm}^{-2}$   $\text{kyr}^{-1}$  during a comparable time span ( $\sim 4$  kyr; Titschack et al., 2015). Combining our new data with mean values from Titschack et al. (2015, 2016), we find an overall correlation of  $R^2 = 0.97$  ( $p < 0.0001$ ) between ARs and on-mound carbonate accumulation rates for CWC mounds (Fig. 5), suggesting that carbonate accumulation is mainly driven by ARs and that the sediment composition plays a subordinate role.

Enhanced mound formation phases with high ARs of  $>100$   $\text{cm kyr}^{-1}$ , as presented above, have been reported from many more CWC mound provinces (when averaged across similar time spans), such as Mauritania (Wienberg et al., 2018; Wienberg et al., 2023), Namibia (Tamborrino et al., 2019), and Scotland (Douarin et al., 2013; Douarin et al., 2014). Based on the correlation we found (Fig. 5), we assume that these CWC mound provinces also accumulate high amounts of carbon(ate). Using a 70 m long MeBo core record, we can for the first time compare carbon(ate) accumulation rates on the same CWC mound at the resolution of individual mound formation phases. This study shows that carbon(ate) accumulation occurred at comparable rates during young and old mound formation phases, making a secondary loss of carbon by diagenetic processes unlikely, and confirms the potential for long-term carbon storage. In addition, the CWC mounds discovered to date are all located

on passive continental margins (cf. Bradley, 2008), further highlighting their potential as very long-term carbon sinks.

### 5.2 The role of sediments in carbon accumulation on CWC mounds

Our results demonstrate that sediments not only are essential for CWC mound formation (Thiem et al., 2006; Wheeler et al., 2007; Roberts et al., 2009; Pirllet et al., 2011; Wang et al., 2021) but also play a substantial role in carbon storage within the mounds, with a contribution of up to 70 % (Table 3). During phases of enhanced CWC mound formation, i.e. high ARs, fast-growing coral frameworks are preserved in an upright position and provide accommodation space and baffling capacity for greater sediment deposition (Wang et al., 2021; see also Dorschel et al., 2007a; Wheeler et al., 2008; Huvenne et al., 2009; Titschack et al., 2009, 2015). This results in mound deposits with low coral and high sediment contents. In contrast, slower-growing CWC frameworks degrade over time, creating a coral rubble layer with less sediment baffling capacity, resulting in mound deposits with high coral and low sediment contents (Titschack et al., 2015, 2016; Wang et al., 2021). However, there are also other factors influencing the contribution of the sedimentary carbon fraction to the total carbon accumulation on a CWC mound. During the enhanced Dragon Mound formation phases (DM5, DM6), the sedimentary carbon fraction dominates the carbon accumulation (it contributes 57 %–70 % to the total carbon accumulation; Table 3), but the most recent mound formation phase documented for BRI ( $BRI_{\text{final}}$ ) shows a relatively lower contribution of 48 % (Tables 2, 3) despite a comparable mound AR. This implies that while carbon(ate) accumulation is steered by ARs, the overall contribution of sedimentary carbon to the total carbon accumulation on a mound can vary when averaging rates over entire mound formation phases. One explanation for this could be that BRI is located slightly deeper and is further away from the coast compared to Dragon Mound: generally, the amount of sediment input increases with proximity to the shore/nearest river mouths (e.g. Diesing, 2020; Epstein et al., 2024).

### 5.3 The role of organic carbon in CWC mounds: a geological perspective

The global Holocene average  $C_{\text{org Acc}}$  for sediment drift deposits globally is  $0.09$  g  $\text{C cm}^{-2}$   $\text{kyr}^{-1}$  (Yin et al., 2024), which is well within the range of our mean  $C_{\text{org Acc}}$  from the off-mound record (see Table 4). This suggests that at the time of mound formation, our off-mound  $C_{\text{org Acc}}$  is representative of a contourite setting that is typical of the hydrodynamic environments surrounding CWC mounds (e.g. Hebbeln et al., 2016).

For the first time, we demonstrate that not only  $C_{\text{inorg}}$  but also  $C_{\text{org Acc}}$  is higher on the CWC mounds studied compared to the adjacent off-mound deposits. This is mostly due

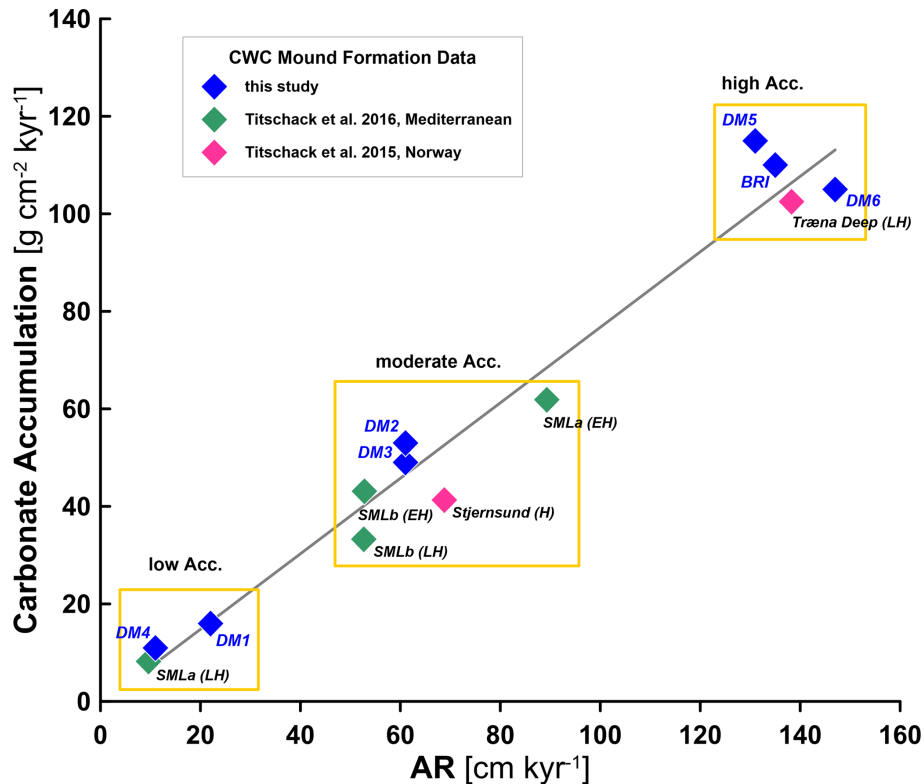


**Figure 5.** Cross-plot outlining the relationship between cold-water coral (CWC) mound aggradation rates (ARs) and the carbonate accumulation rate with  $R^2 = 0.97$  ( $p < 0.0001$ ) for mean rates calculated for individual mound formation phases or, if not available, formation units covering time spans of  $>3$  kyr and minimum ARs of  $>5$  cm kyr<sup>-1</sup>.  $n = 13$ . Blue symbols are from this study; green symbols are from Titschack et al. (2016), with two cores from the Ionian Sea (Santa Maria di Leuca (SML) a) and b); and the pink symbols are from Titschack et al. (2015) Norway. For the literature data, the approximate time period of the mound formation records is given in brackets: entire (H), early (EH), or late (LH) Holocene.

to a higher AR of CWC mound deposits. However, independent of the AR, we found a higher sediment  $C_{org}$  wt % content on the mounds compared to the sediment of the adjacent seafloor (off-mound), greater by a factor of 1.2–1.4 (Table 4). This indicates that not only does the  $C_{org}$  accumulate faster on the mounds but the material deposited on the mounds itself has a different composition and is enriched with  $C_{org}$ . Irrespective of the quantity of sediment deposition, the  $C_{org}$  fraction of a sedimentary unit on the mound is higher, meaning that the on-mound matrix sediments are selectively enriched with  $C_{org}$ . Thus, CWC mounds are effective sinks of  $C_{org}$  due to (1) the higher CWC mound ARs compared to sedimentation rates on the adjacent seafloor and (2) selective enrichment of the mound matrix sediments with  $C_{org}$ .

While CWC mounds are generally located in areas of high bottom currents (Mienis et al., 2007; Dorschel et al., 2009; Hebbeln et al., 2016), the coral framework itself locally reduces the regional flow speed by up to 70%; changes the carrying capacity of the water mass; and allows the deposition of suspended, fine-grained, and lighter sediment particles between the corals (Bartzke et al., 2021; Wang et al., 2021). There is a link between the fining of sediments and

an increase in  $C_{org}$  content (e.g. Dahl et al., 2016; Paradis et al., 2023), which has also been observed on CWC mounds (Kiriakoulakis et al., 2007; Stalder et al., 2018). This suggests that despite strong bottom currents,  $C_{org}$ -rich particles (large surface area per weight, low density; Bergamaschi et al., 1997; Paradis et al., 2023) were trapped on the mound through the baffling effect of the coral framework (Wang et al., 2021; Corbera et al., 2022), while at the same time, the adjacent (off-mound) seafloor faced a sediment bypass situation (sensu Wang et al., 2021). In addition, pycnocline-related nepheloid layers carried by internal waves certainly play a role in the transport of  $C_{org}$  across the Alborán Sea (Masqué et al., 2003; Puig et al., 2004; Sanchez-Vidal et al., 2005) and have been widely attributed to the occurrence of CWCs and mounds (Frederiksen et al., 1992; Mienis et al., 2007; Hanz et al., 2019). Following this concept, Wang et al. (2019) and Corbera et al. (2021) also suggested internal waves as a key control of CWC reef development within the southern Alborán Sea by delivering  $C_{org}$ -rich materials as food to the corals on CWC mounds at certain depth intervals. Ultimately, it is currently unclear whether the selective enrichment of  $C_{org}$  within the mound records is caused by neph-

eloid layer formation and/or a  $C_{\text{org}}$  bypass situation in the off-mound setting. Large CWC mounds forming significant elevations on the seafloor can also self-induce local downward transport of organic matter towards the mound summit (Mohn et al., 2014; Cyr et al., 2016; Soetaert et al., 2016; van der Kaaden et al., 2021), which may further contribute to a higher  $C_{\text{org}}$  supply to mounds compared to the plain seafloor.

Notably, it is the combination of (i) the physical hydrodynamic processes outlined here and (ii) biological processes that controls the  $C_{\text{org}}$  Acc on a CWC mound. Both processes happen at two scales: at a larger hydrodynamic scale,  $C_{\text{org}}$  is delivered to the reef by currents, while the baffling of  $C_{\text{org}}$  happens at the scale of the coral frameworks on the mound. From a biological perspective,  $C_{\text{org}}$  is produced at a large scale by primary ( $C_{\text{org}}$ ) production in the surface ocean, and after being supplied to the CWC mound, biological processes at the local scale of the reef further determine how much  $C_{\text{org}}$  eventually gets accumulated. Thriving CWC reefs are highly productive and are considered hotspots of biomass, metabolism, and  $C_{\text{org}}$  turnover (van Oevelen et al., 2009; Cathalot et al., 2015; De Clippele et al., 2021a; De Clippele et al., 2021b). This includes further recycling of organic waste products within the CWC reef's food web (Maier et al., 2020, 2023). As primary-production-derived  $C_{\text{org}}$  is exclusively respired or transformed but not newly produced by the heterotroph CWC reef fauna,  $C_{\text{org}}$  accumulation in a CWC mound should be lower compared to off-mound deposits. Accordingly, high-level metabolism (i.e. higher carbon turnover relative to the surrounding seafloor; de Froe et al., 2019; De Clippele et al., 2021a) within the reef framework may reduce the amount of  $C_{\text{org}}$  available for accumulation in the sediment (Wehrmann et al., 2009). This is in contrast to our finding that CWC mound sediment deposits are enriched in  $C_{\text{org}}$  and have higher  $C_{\text{org}}$  Acc rates compared to the off-mound deposits. Two studies on CWC reef surface sediments (northeast Atlantic) also found a  $C_{\text{org}}$  wt % enriched top layer relative to an off-mound setting (Kiriakoulakis et al., 2004; de Froe et al., 2019). Consequently, the sediments arriving at the CWC mound may initially have an even higher  $C_{\text{org}}$  enrichment, but the CWC reef fauna prevents part of it from being buried in the long term. On the other hand, other benthic ecosystems characterised by high biodiversity and species density exhibit enhanced levels of  $C_{\text{org}}$ -rich detritus, bioturbation, etc., which may also increase the quantity of  $C_{\text{org}}$  buried (Canfield, 1994; Karlson et al., 2010; Strong et al., 2015; James et al., 2024). However, it is unknown what role these processes play in CWC reefs. This all emphasises that the complex interplay between biological and geological processes on CWC mounds, especially regarding  $C_{\text{org}}$  burial, is poorly understood and poorly quantified.

## 5.4 Cold-water coral mounds as carbon sinks

Carbon sinks are natural systems that remove carbon from the atmosphere–hydrosphere carbon cycle and store it in the bio- or lithosphere (see Baker, 2007; Howard et al., 2017; Cartapanis et al., 2018). CWC mounds transfer carbon from the short-term carbon cycle (atmosphere–hydrosphere) to the long-term carbon cycle (lithosphere). While the  $C_{\text{inorg}}$  sink removes dissolved inorganic carbon from the surrounding water mass, the  $C_{\text{org}}$  sink relies on  $C_{\text{org}}$  production in the surface ocean (primary production) and thus removes carbon from the surface ocean. Consequently, both carbon sinks remove carbon from different short-term reservoirs.

Our study provides quantitative evidence that the burial of both  $C_{\text{inorg}}$  and  $C_{\text{org}}$  happens at enhanced rates on CWC mounds. More specifically, we found that during the same period, total carbon accumulation on two Mediterranean CWC mounds exceeds the rates of the adjacent seafloor by a factor of 14–19 during the same period. For  $C_{\text{inorg}}$  Acc (carbonate) individually, a factor of 15–19 results from our record, confirming that CWC mounds are effective local carbonate factories. As a novelty, this study highlights the additional importance of CWC mounds as long-term sinks for  $C_{\text{org}}$ . The accumulation of  $C_{\text{org}}$  is 9–14 times higher on the CWC mounds due to not only the enhanced sediment deposition within the mounds but also higher  $C_{\text{org}}$  content of the deposited sediment.

In addition to comparing carbon accumulation rates during the mound formation phases, assessing the total long-term net carbon burial throughout a mound's entire existence (i.e. Dragon Mound,  $\sim 400$  kyr) in both on- and off-mound settings may provide further insight into the potential role of CWC mounds in the marine carbon cycle. Notably, there were extensive periods without any mound formation or carbon accumulation (see hiatuses in Fig. 3), whereas off-mound accumulation is expected to be continuous. However, our off-mound record is comparably short ( $\sim 126$  kyr) and only overlaps with one mound formation phase on Dragon Mound. A stratigraphically longer off-mound record, preferably spanning the full record of Dragon Mound from initiation until present, would allow a much more meaningful comparison. Sediment core records documenting  $\sim 400$  kyr of carbon accumulation are scarce in the southern Alborán Sea. The only available off-mound sediment core record that provides the necessary data is ODP Leg 161 Hole 979A (Comas et al., 1996; Shipboard Scientific Party, 1996) at 1062 m b.s.l. ( $35^{\circ}43.427' \text{ N}$ ,  $3^{\circ}12.353' \text{ W}$ ; data sources are <https://web.iodp.tamu.edu/OVERVIEW/?&exp=161&site=979>, last access: 28 April 2025 and the biostratigraphic age model from de Kaenel et al., 1999).

To assess the applicability of this ODP core as a valuable off-mound counterpart to our on-mound record from Dragon Mound, we first compare it to the off-mound record analysed in this study. Over the last  $>100$  kyr, the off-mound record presented herein (orig-

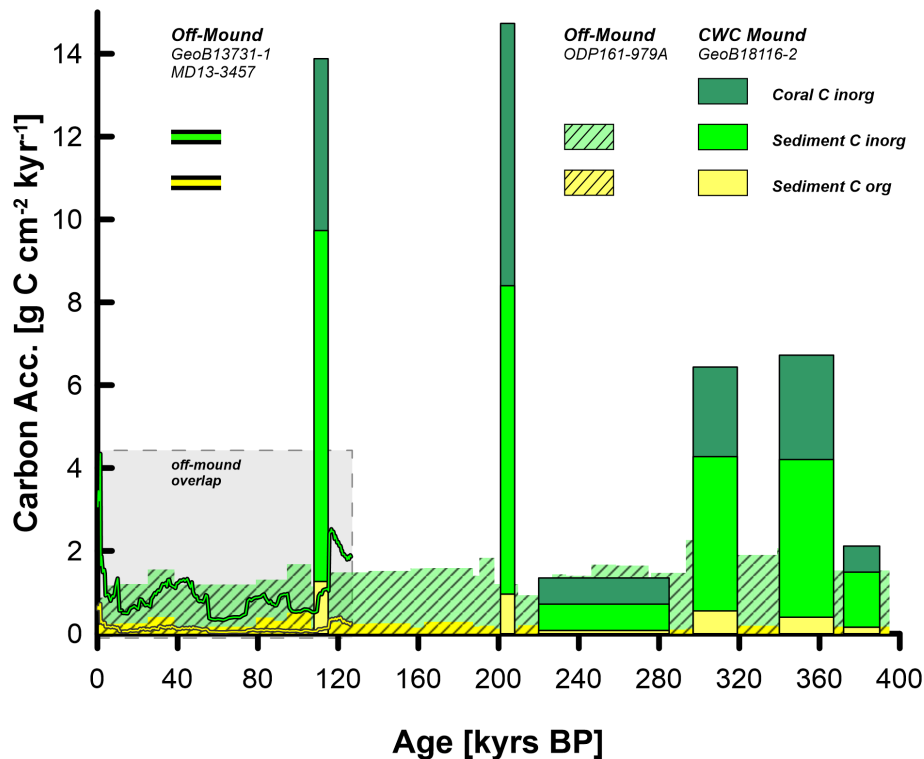


**Figure 6.** Long-term comparison of on- and off-mound carbon accumulation in the southern Alborán Sea. The off-mound data are derived from our off-mound cores GeoB13731-1 and MD13-3457, together spanning the last  $\sim 126$  kyr, and core ODP161-979A, spanning the last 400 kyr (the overlap between both records is marked by the grey box). On-mound carbon accumulation is from Dragon Mound (GeoB18116-2). Carbon accumulation for all records is divided into its different fractions: coral inorganic carbon (coral C inorg) and sediment inorganic and organic carbon (sediment C inorg and sediment C org). Carbon accumulation rates are stacked as cumulative values.

inating from cores GeoB13731-1 and MD13-3457), with a mean organic carbon accumulation rate of  $0.2 \text{ g C}_{\text{org}} \text{ cm}^{-2} \text{ kyr}^{-1}$  (range:  $0.03\text{--}0.7 \text{ g C}_{\text{org}} \text{ cm}^{-2} \text{ kyr}^{-1}$ ), is comparable to the  $0.3 \text{ g C}_{\text{org}} \text{ cm}^{-2} \text{ kyr}^{-1}$  (range:  $0.1\text{--}0.5 \text{ g C}_{\text{org}} \text{ cm}^{-2} \text{ kyr}^{-1}$ ) in the ODP core. Similarly, the mean inorganic carbon accumulation of  $0.9 \text{ g C}_{\text{inorg}} \text{ cm}^{-2} \text{ kyr}^{-1}$  (range:  $0.3\text{--}3.6 \text{ g C}_{\text{inorg}} \text{ cm}^{-2} \text{ kyr}^{-1}$ ) at our off-mound site is very close to the  $1.0 \text{ g C}_{\text{inorg}} \text{ cm}^{-2} \text{ kyr}^{-1}$  (range:  $0.7\text{--}1.3 \text{ g C}_{\text{inorg}} \text{ cm}^{-2} \text{ kyr}^{-1}$ ) in the ODP core. Consequently, the mean total carbon accumulation rates in both cores are also quite similar:  $1.1 \text{ g C cm}^{-2} \text{ kyr}^{-1}$  (range:  $0.3\text{--}4.3 \text{ g C cm}^{-2} \text{ kyr}^{-1}$ ) and  $1.3 \text{ g C cm}^{-2} \text{ kyr}^{-1}$  (range:  $0.9\text{--}1.7 \text{ g C cm}^{-2} \text{ kyr}^{-1}$ ), respectively, highlighting the regional consistency of off-mound net carbon burial through time. Correspondingly, our off-mound core record represents not only local but also regional off-mound accumulation dynamics that are well-suited to the purpose of this study.

Finally, the integration of net carbon burial for on- and off-mound records (GeoB18116-2 versus ODP161-979A, respectively) over the complete evolution of Dragon Mound since mound initiation, i.e. the last  $\sim 400$  kyr covering several glacial–interglacial cycles, reveals that total carbon accumulation at Dragon Mound ( $649 \text{ g C cm}^{-2}$ ) is 20% higher than at the off-mound site ODP161-979A ( $544 \text{ g C cm}^{-2}$ ;

Fig. 6). Importantly, this is observed despite  $>200$  kyr of non-sedimentation on the mound. In this direct comparison, the extensive BRI<sub>final</sub> mound formation phase, which is widely recorded in the EMCP (see Wienberg et al., 2022), cannot be considered, as it is not documented at Dragon Mound. Thus, for other CWC mounds in the EMCP, the surplus on-mound carbon accumulation might be even higher.

From a broader perspective, the carbon and carbonate accumulation on the CWC mounds investigated corresponds well with other ecosystems that have been attributed a relevant role in the carbon cycle. The mean carbonate accumulation rates of  $105\text{--}115 \text{ g CaCO}_3 \text{ cm}^{-2} \text{ kyr}^{-1}$  during the last three enhanced mound formation phases at BRI and Dragon Mound are similar to those of tropical coral reefs (mean of  $\sim 120 \text{ g CaCO}_3 \text{ cm}^{-2} \text{ kyr}^{-1}$ ; Milliman, 1993). When looking at total carbon accumulation, the CWC mounds studied accumulate  $\sim 1\text{--}15 \text{ g C cm}^{-2} \text{ kyr}^{-1}$  during phases of active mound formation, while carbon storing ecosystems like peatlands accumulate carbon at a rate of  $1.4\text{--}2.2 \text{ g C cm}^{-2} \text{ kyr}^{-1}$  (Roulet et al., 2007), seagrass meadows at  $\sim 3.6 \text{ g C cm}^{-2} \text{ kyr}^{-1}$  (Samper-Villarreal et al., 2018; export production not considered), and salt marshes at  $\sim 4.0 \text{ g C cm}^{-2} \text{ kyr}^{-1}$  (Johnson et al., 2007). These examples outline the capacity of CWC mounds to temporarily accumu-

late carbon at similar or even higher rates compared to other, well-known carbon storing ecosystems.

## 6 Conclusion

This study presents a first calculation of the total carbon accumulation, including inorganic ( $C_{\text{inorg}}$ ) and organic carbon ( $C_{\text{org}}$ ), on two CWC mounds in the western Mediterranean (Alborán Sea), showing that active CWC mounds can be effective carbon sinks across geological timescales. During times of enhanced mound formation with mound ARs of  $>100 \text{ cm kyr}^{-1}$ , the total carbon accumulation is  $\sim 15 \text{ g C cm}^{-2} \text{ kyr}^{-1}$  and is estimated to be 14–19 times higher than in the adjacent seafloor deposits during the same time period. We highlight that CWC mounds effectively act as local carbon sinks for both  $C_{\text{inorg}}$  and  $C_{\text{org}}$  during mound formation phases and most likely beyond. Moreover, CWC mounds accumulate carbon at a similar level to that of other ecosystems, e.g. salt marshes, seagrass meadows, or peatlands, that are known for their high carbon-storing capacity. We find that high carbonate accumulation rates correlate with high mound ARs. With multiple known CWC mound provinces exhibiting high ARs of  $>100 \text{ cm kyr}^{-1}$ , we speculate that CWC mounds may play a vital role in the carbon budget of many regions. However, more studies on the role of CWC mounds in the long-term carbon cycle and on the dynamics of carbon accumulation across time and space are needed to validate this. Knowledge about the distribution and abundance of CWC mounds along the world's continental margins is still very limited, hindering further upscaling at present.

With our data, we underline that the contribution of sedimentary carbon is crucial to the process of on-mound carbon accumulation. Furthermore, sediment-derived  $C_{\text{org}}$  may play a previously overlooked, important role in on-mound carbon accumulation, and our data suggest that CWC mound sediments may be selectively enriched in  $C_{\text{org}}$ .  $C_{\text{org}}$  contributes 6%–9% to total carbon accumulation on the CWC mounds studied and needs to be considered when evaluating the carbon accumulation of marine carbonate factories.

Through an analysis of a total time span of  $\sim 400 \text{ kyr}$  and the investigation of all major compartments of carbon accumulation, this study provides a step towards including CWC mounds in global marine carbon budget assessments. On that note, an increasing number of studies highlight the overlooked role that marine fauna and heterotroph ecosystems as a whole play in transferring carbon between different carbon reservoirs (i.e. atmosphere, hydrosphere, biosphere, and lithosphere; Schmitz et al., 2014; Schmitz et al., 2018; James et al., 2024).

*Data availability.* All previously unpublished raw data are made available through the open-access data repository and the World Data Center PANGAEA. This includes the sediment density measurements of cores MD13-3457 (Greiffenhagen et al., 2025a, <https://doi.org/10.1594/PANGAEA.971923>) and GeoB18116-2 (Greiffenhagen et al., 2025b, <https://doi.org/10.1594/PANGAEA.971884>). Further, stable oxygen isotope data from MD13-3457 were made available (Greiffenhagen et al., 2025c, <https://doi.org/10.1594/PANGAEA.971935>), as well as the determined AMS  $^{14}\text{C}$  ages (Greiffenhagen et al., 2025d, <https://doi.org/10.1594/PANGAEA.971925>) and TIC/TOC data (Greiffenhagen et al., 2025e, <https://doi.org/10.1594/PANGAEA.971806>). TIC/TOC data are also published for on-mound core GeoB16118-2 (Greiffenhagen et al., 2025f, <https://doi.org/10.1594/PANGAEA.971862>). Further, the CT data of core GeoB16118-2 are made available in raw DICOM format (Greiffenhagen et al., 2025g, <https://doi.org/10.1594/PANGAEA.973154>), as well as in processed format, showing the coral and sediment volumes within Dragon Mound (Greiffenhagen et al., 2025h, <https://doi.org/10.1594/PANGAEA.971900>).

*Supplement.* The supplement related to this article is available online at <https://doi.org/10.5194/bg-22-2201-2025-supplement>.

*Author contributions.* DH conceptualised the study; JT and LG designed the methodology. DH and CW organised the data collection and conducted the fieldwork. JT and LG performed the computed tomography measurements. HW contributed further data sets to the study. LG conducted the formal analysis and wrote the original draft. All authors were involved in the interpretation of the results, the revision, and the writing of the final version of the paper.

*Competing interests.* The contact author has declared that none of the authors has any competing interests.

*Disclaimer.* Publisher's note: Copernicus Publications remains neutral with regard to jurisdictional claims made in the text, published maps, institutional affiliations, or any other geographical representation in this paper. While Copernicus Publications makes every effort to include appropriate place names, the final responsibility lies with the authors.

*Acknowledgements.* We would like to thank the Klinikum Bremen-Mitte, Christian Timann, and Arne-Jörn Lemke for providing their facilities and their help for the computed tomographies performed. The GeoB Core Repository at the MARUM (University of Bremen, Germany) is acknowledged for providing sediment cores and sample material. We are grateful for the support from Brit Kokisch, Christina Gnade, and Timo Fleischmann (University of Bremen, Germany) during sampling and TIC/TOC and dry bulk density measurements. We kindly acknowledge the Poznan Radiocarbon Laboratory, Poland, for performing AMS  $^{14}\text{C}$  radiocarbon dating, as well as Henning Kuhnert and Birgit Meyer-Schack (MARUM) for

their lab support during the stable isotope measurements. Further, onboard assistance by the MeBo team of the MARUM Center for Marine Environmental Sciences and the captain, crew, technicians, and scientists of the R/V *Poseidon* cruise POS385, R/V *Maria S. Merian* cruise MSM36, and R/V *Marion Dufresne* cruise MD194 are gratefully acknowledged. Finally, the editor, Niels de Winter, Vrije Universiteit Amsterdam, and the two reviewers, Evan Edinger, Memorial University of Newfoundland, and Kristina Beck, University of Edinburgh, for their comments that have greatly improved this paper.

**Financial support.** This research has been supported by the Deutsche Forschungsgemeinschaft (grant no. EXC 2077) and The Ocean Floor – Earth’s Uncharted Interface (grant no. 390741603).

The article processing charges for this open-access publication were covered by the University of Bremen.

**Review statement.** This paper was edited by Niels de Winter and reviewed by Kristina Beck and Evan Edinger.

## References

- Álvarez, M., Catalá, T. S., Civitarese, G., Coppola, L., Hasoun, A. E. R., Ibello, V., Lazzari, P., Lefevre, D., Macías, D., Santinelli, C., and Ulses, C.: Mediterranean Sea general biogeochemistry, in: *Oceanography of the Mediterranean Sea*, edited by: Schroeder, K. and Chiggiato, J., Elsevier, 387–451, <https://doi.org/10.1016/B978-0-12-823692-5.00004-2>, 2023.
- Baker, D. F.: Reassessing Carbon Sinks, *Science*, 317, 1708–1709, <https://doi.org/10.1126/science.1144863>, 2007.
- Bartzke, G., Siemann, L., Büssing, R., Nardone, P., Koll, K., Hebbeln, D., and Huhn, K.: Investigating the Prevailing Hydrodynamics Around a Cold-Water Coral Colony Using a Physical and a Numerical Approach, *Front. Mar. Sci.*, 8, 663304, <https://doi.org/10.3389/fmars.2021.663304>, 2021.
- Bergamaschi, B. A., Tsamakidis, E., Keil, R. G., Eglinton, T. I., Montluçon, D. B., and Hedges, J. I.: The effect of grain size and surface area on organic matter, lignin and carbohydrate concentration, and molecular compositions in Peru Margin sediments, *Geochim. Cosmochim. Ac.*, 61, 1247–1260, [https://doi.org/10.1016/S0016-7037\(96\)00394-8](https://doi.org/10.1016/S0016-7037(96)00394-8), 1997.
- Blum, P.: *Physical Properties Handbook: A Guide to the Shipboard Measurement of Physical Properties of Deep-Sea Cores*, College Station, Texas, USA, <http://www-odp.tamu.edu> (last access: 28 April 2025), 1997.
- Bradley, D. C.: Passive margins through earth history, *Earth-Sci. Rev.*, 91, 1–26, <https://doi.org/10.1016/j.earscirev.2008.08.001>, 2008.
- Burdige, D. J.: Preservation of Organic Matter in Marine Sediments: Controls, Mechanisms, and an Imbalance in Sediment Organic Carbon Budgets?, *Chem. Rev.*, 107, 467–485, <https://doi.org/10.1021/cr050347q>, 2007.
- Butzin, M., Köhler, P., and Lohmann, G.: Marine radiocarbon reservoir age simulations for the past 50,000 years, *Geophys. Res. Lett.*, 44, 8473–8480, <https://doi.org/10.1002/2017gl074688>, 2017.
- Canfield, D. E.: Factors influencing organic carbon preservation in marine sediments, *Chem. Geol.*, 114, 315–329, [https://doi.org/10.1016/0009-2541\(94\)90061-2](https://doi.org/10.1016/0009-2541(94)90061-2), 1994.
- Camoin, G. F. and Webster, J. M.: Coral reef response to Quaternary sea-level and environmental changes: State of the science, *Sedimentology*, 62, 401–428, <https://doi.org/10.1111/sed.12184>, 2015.
- Cartapanis, O., Galbraith, E. D., Bianchi, D., and Jaccard, S. L.: Carbon burial in deep-sea sediment and implications for oceanic inventories of carbon and alkalinity over the last glacial cycle, *Clim. Past*, 14, 1819–1850, <https://doi.org/10.5194/cp-14-1819-2018>, 2018.
- Cathalot, C., Van Oevelen, D., Cox, T. J. S., Kutti, T., Lavaleye, M., Duineveld, G., and Meysman, F. J. R.: Cold-water coral reefs and adjacent sponge grounds: hotspots of benthic respiration and organic carbon cycling in the deep sea, *Front. Mar. Sci.*, 2, 00037, <https://doi.org/10.3389/fmars.2015.00037>, 2015.
- Comas, M. C., Zahn, R., Klaus, A., et al.: Leg 161, Proc. ODP, Init. Repts., College Station, TX (Ocean Drilling Program). <https://doi.org/10.2973/odp.proc.ir.161.1996>, 1996.
- Corbera, G., Lo Iacono, C., Gràcia, E., Grinyó, J., Pierdomenico, M., Huvenne, V. A. I., Aguilar, R., and Gili, J. M.: Ecological characterisation of a Mediterranean cold-water coral reef: Cabliers Coral Mound Province (Alboran Sea, western Mediterranean), *Prog. Oceanogr.*, 175, 245–262, <https://doi.org/10.1016/j.pocean.2019.04.010>, 2019.
- Corbera, G., Lo Iacono, C., Standish, C. D., Anagnostou, E., Titschack, J., Katsamenis, O., Cacho, I., Van Rooij, D., Huvenne, V. A. I., and Foster, G. L.: Glacio-eustatic variations and sapropel events as main controls on the Middle Pleistocene-Holocene evolution of the Cabliers Coral Mound Province (W Mediterranean), *Quat. Sci. Rev.*, 253, 106783, <https://doi.org/10.1016/j.quascirev.2020.106783>, 2021.
- Corbera, G., Lo Iacono, C., Simarro, G., Grinyó, J., Ambroso, S., Huvenne, V. A. I., Mienis, F., Carreiro-Silva, M., Martins, I., Mano, B., Orejas, C., Larsson, A., Hennige, S., and Gori, A.: Local-scale feedbacks influencing cold-water coral growth and subsequent reef formation, *Sci. Rep.*, 12, 20389, <https://doi.org/10.1038/s41598-022-24711-7>, 2022.
- Cyr, F., van Haren, H., Mienis, F., Duineveld, G., and Bourgault, D.: On the influence of cold-water coral mound size on flow hydrodynamics, and vice versa, *Geophys. Res. Lett.*, 43, 775–783, <https://doi.org/10.1002/2015GL067038>, 2016.
- Dahl, M., Deyanova, D., Gutschow, S., Asplund, M. E., Lyimo, L. D., Karamfilov, V., Santos, R., Bjork, M., and Gullstrom, M.: Sediment Properties as Important Predictors of Carbon Storage in *Zostera marina* Meadows: A Comparison of Four European Areas, *PLoS One*, 11, e0167493, <https://doi.org/10.1371/journal.pone.0167493>, 2016.
- Davies, A. J. and Guinotte, J. M.: Global habitat suitability for framework-forming cold-water corals, *PLoS One*, 6, e18483, <https://doi.org/10.1371/journal.pone.0018483>, 2011.
- De Clippele, L. H., Rovelli, L., Ramiro-Sánchez, B., Kazanidis, G., Vad, J., Turner, S., Glud, R. N., and Roberts, J. M.: Mapping cold-water coral biomass: an approach to derive ecosystem functions, *Coral Reefs*, 40, 215–231, <https://doi.org/10.1007/s00338-020-02030-5>, 2021a.

- De Clippele, L. H., van der Kaaden, A.-S., Maier, S. R., de Froe, E., and Roberts, J. M.: Biomass Mapping for an Improved Understanding of the Contribution of Cold-Water Coral Carbonate Mounds to C and N Cycling, *Front. Mar. Sci.*, 8, 721062, <https://doi.org/10.3389/fmars.2021.721062>, 2021b.
- de Froe, E., Rovelli, L., Glud, R. N., Maier, S. R., Duineveld, G., Mienis, F., Lavaley, M., and van Oevelen, D.: Benthic Oxygen and Nitrogen Exchange on a Cold-Water Coral Reef in the North-East Atlantic Ocean, *Front. Mar. Sci.*, 6, 00665, <https://doi.org/10.3389/fmars.2019.00665>, 2019.
- de Haas, H., Mienis, F., Frank, N., Richter, T. O., Steinacher, R., de Stigter, H., van der Land, C., and van Weering, T. C. E.: Morphology and sedimentology of (clustered) cold-water coral mounds at the south Rockall Trough margins, NE Atlantic Ocean, *Facies*, 55, 1–26, <https://doi.org/10.1007/s10347-008-0157-1>, 2009.
- de Kaenel, E., Siesser, W. G., and Murat, A.: Pleistocene calcareous nannofossil biostratigraphy and the western Mediterranean sapropels, Sites 974 to 977 and 979, in: Leg 161, Proc. ODP, Sci. Res., edited by: Zahn, R., Comas, M. C., and Klaus, A., College Station, TX (Ocean Drilling Program), 159–183, <https://doi.org/10.2973/odp.proc.sr.161.250.1999>, 1999.
- Diesing, M.: Deep-sea sediments of the global ocean, *Earth Syst. Sci. Data*, 12, 3367–3381, <https://doi.org/10.5194/essd-12-3367-2020>, 2020.
- Dorschel, B., Hebbeln, D., Rüggeberg, A., Dullo, W., and Freiwald, A.: Growth and erosion of a cold-water coral covered carbonate mound in the Northeast Atlantic during the Late Pleistocene and Holocene, *Earth Planet. Sci. Lett.*, 233, 33–44, <https://doi.org/10.1016/j.epsl.2005.01.035>, 2005.
- Dorschel, B., Hebbeln, D., Foubert, A., White, M., and Wheeler, A. J.: Hydrodynamics and cold-water coral facies distribution related to recent sedimentary processes at Galway Mound west of Ireland, *Mar. Geol.*, 244, 184–195, <https://doi.org/10.1016/j.margeo.2007.06.010>, 2007a.
- Dorschel, B., Hebbeln, D., Rüggeberg, A., and Dullo, C.: Carbonate budget of a cold-water coral carbonate mound: Propeller Mound, Porcupine Seabight, *Int. J. Earth Sci.*, 96, 73–83, <https://doi.org/10.1007/s00531-005-0493-0>, 2007b.
- Dorschel, B., Wheeler, A. J., Huvenne, V. A. I., and de Haas, H.: Cold-water coral mounds in an erosive environment setting: TOBI side-scan sonar data and ROV video footage from the northwest Porcupine Bank, NE Atlantic, *Mar. Geol.*, 264, 218–229, <https://doi.org/10.1016/j.margeo.2009.06.005>, 2009.
- Douarin, M., Elliot, M., Noble, S. R., Sinclair, D., Henry, L.-A., Long, D., Moreton, S. G., and Roberts, J. M.: Growth of north-east Atlantic cold-water coral reefs and mounds during the Holocene: A high resolution U-series and  $^{14}\text{C}$  chronology, *Earth Planet. Sci. Lett.*, 375, 176–187, <https://doi.org/10.1016/j.epsl.2013.05.023>, 2013.
- Douarin, M., Sinclair, D. J., Elliot, M., Henry, L.-A., Long, D., Mitchison, F., and Roberts, J. M.: Changes in fossil assemblage in sediment cores from Mingulay Reef Complex (NE Atlantic): Implications for coral reef build-up, *Deep Sea Res. Pt. II: Top. Stud. Oceanogr.*, 99, 286–296, <https://doi.org/10.1016/j.dsr2.2013.07.022>, 2014.
- Duchesne, M. J., Moore, F., Long, B. F., and Labrie, J.: A rapid method for converting medical Computed Tomography scanner topogram attenuation scale to Hounsfield Unit scale and to obtain relative density values, *Eng. Geol.*, 103, 100–105, <https://doi.org/10.1016/j.enggeo.2008.06.009>, 2009.
- Edinger, E., Bourillet, J.-F., Menot, L., Lartaud, F., Chemel, M., and Jorry, S.: Late Holocene and recent cold-water coral calcium carbonate production in Guilvinec Canyon, Bay of Biscay, France. *Deep Sea Res. Pt. II: Top. Stud. Oceanogr.*, 220, 105451, <https://doi.org/10.1016/j.dsr2.2024.105451>, 2025.
- EMODnet Bathymetry Consortium: EMODnet Digital Bathymetry (DTM 2022), EMODnet [data set], <https://doi.org/10.12770/ff3aff8a-cff1-44a3-a2c8-1910bf109f85>, 2022.
- Epstein, G., Fuller, S. D., Hingmire, D., Myers, P. G., Peña, A., Pennelly, C., and Baum, J. K.: Predictive mapping of organic carbon stocks in surficial sediments of the Canadian continental margin, *Earth Syst. Sci. Data*, 16, 2165–2195, <https://doi.org/10.5194/essd-16-2165-2024>, 2024.
- Ercilla, G., Juan, C., Hernandez-Molina, F. J., Bruno, M., Estrada, F., Alonso, B., Casas, D., Farran, M. L., Llave, E., García, M., Vázquez, J. T., D’Acremont, E., Gorini, C., Palomino, D., Valencia, J., El Moumni, B., and Ammar, A.: Significance of bottom currents in deep-sea morphodynamics: an example from the Alboran Sea, *Mar. Geol.*, 378, 157–170, <https://doi.org/10.1016/j.margeo.2015.09.007>, 2016.
- Fentimen, R., Feenstra, E., Rüggeberg, A., Vennemann, T., Hajdas, I., Adatte, T., Van Rooij, D., and Foubert, A.: Cold-Water Coral Mound Archive Provides Unique Insights Into Intermediate Water Mass Dynamics in the Alboran Sea During the Last Deglaciation, *Front. Mar. Sci.*, 7, 00354, <https://doi.org/10.3389/fmars.2020.00354>, 2020.
- Fentimen, R., Feenstra, E., Rüggeberg, A., Hall, E., Rime, V., Vennemann, T., Hajdas, I., Rosso, A., Van Rooij, D., Adatte, T., Vogel, H., Frank, N., and Foubert, A.: A 300 000-year record of cold-water coral mound build-up at the East Melilla Coral Province (SE Alboran Sea, western Mediterranean), *Clim. Past*, 18, 1915–1945, <https://doi.org/10.5194/cp-18-1915-2022>, 2022.
- Fentimen, R., Feenstra, E. J., Rüggeberg, A., Hall, E., Rosso, A., Hajdas, I., Jaramillo-Vogel, D., Grobety, B., Adatte, T., Van Rooij, D., Frank, N., and Foubert, A.: Staggered cold-water coral mound build-up on an Alboran ridge during the last deglacial (East Melilla Mound Field, western Mediterranean), *Mar. Geol.*, 457, 106994, <https://doi.org/10.1016/j.margeo.2023.106994>, 2023.
- Fink, H. G., Wienberg, C., De Pol-Holz, R., Wintersteller, P., and Hebbeln, D.: Cold-water coral growth in the Alboran Sea related to high productivity during the Late Pleistocene and Holocene, *Mar. Geol.*, 339, 71–82, <https://doi.org/10.1016/j.margeo.2013.04.009>, 2013.
- Frank, N., Ricard, E., Lutringer-Paquet, A., van der Land, C., Colin, C., Blamart, D., Foubert, A., Van Rooij, D., Henriot, J.-P., de Haas, H., and van Weering, T.: The Holocene occurrence of cold-water corals in the NE Atlantic: Implications for coral carbonate mound evolution, *Mar. Geol.*, 266, 129–142, <https://doi.org/10.1016/j.margeo.2009.08.007>, 2009.
- Frederiksen, R., Jensen, A., and Westerberg, H.: The distribution of the scleractinian coral *Lophelia pertusa* around the Faroe Islands and the relation to internal tidal mixing, *Sarsia*, 77, 157–171, <https://doi.org/10.1080/00364827.1992.10413502>, 1992.
- Freudenthal, T. and Wefer, G.: Drilling cores on the sea floor with the remote-controlled sea floor drilling rig

- MeBo, *Geosci. Instrum. Method. Data Syst.*, 2, 329–337, <https://doi.org/10.5194/gi-2-329-2013>, 2013.
- GEBCO Bathymetric Compilation Group: The GEBCO\_2024 Grid – a continuous terrain model of the global oceans and land, NERC EDS British Oceanographic Data Centre [data set], <https://doi.org/10.5285/1c44ce99-0a0d-5f4f-e063-7086abc0ea0f>, 2024.
- Gerland, S. and Villinger, H.: Nondestructive density determination on marine sediment cores from gamma-ray attenuation measurements, *Geo-Marine Letters*, 15, 111–118, <https://doi.org/10.1007/BF01275415>, 1995.
- Greiffenhagen, L., Titschack, J., Wienberg, C., Wang, H., and Hebbeln, D.: Sediment density measurements based on pycnometer measurements of core MD13-3457 from the Alborán Sea, Marion Dufresne Cruise MD194, PANGAEA [data set], <https://doi.org/10.1594/PANGAEA.971923>, 2025a.
- Greiffenhagen, L., Titschack, J., Wienberg, C., Wang, H., and Hebbeln, D.: Sediment density measurements based on pycnometer and CT measurements of sediment core GeoB18116-2 from Dragon Mound, Alborán Sea, Maria S. Merian cruise MSM36, PANGAEA [data set], <https://doi.org/10.1594/PANGAEA.971884>, 2025b.
- Greiffenhagen, L., Titschack, J., Wienberg, C., Wang, H., and Hebbeln, D.: Stable oxygen isotopes of *Cibicides mundulus* from sediment core MD13-3457, Alborán Sea, Marion Dufresne Cruise MD194, PANGAEA [data set], <https://doi.org/10.1594/PANGAEA.971935>, 2025c.
- Greiffenhagen, L., Titschack, J., Wienberg, C., Wang, H., and Hebbeln, D.: AMS 14C age determination for sediment core MD13-3457, Alborán Sea, Marion Dufresne Cruise MD194, PANGAEA [data set], <https://doi.org/10.1594/PANGAEA.971925>, 2025d.
- Greiffenhagen, L., Titschack, J., Wienberg, C., Wang, H., and Hebbeln, D.: Total Organic Carbon and Total Inorganic Carbon content data of sediment core MD13-3457, Alborán Sea, Marion Dufresne Cruise MD194, PANGAEA [data set], <https://doi.org/10.1594/PANGAEA.971806>, 2025e.
- Greiffenhagen, L., Titschack, J., Wienberg, C., Wang, H., and Hebbeln, D.: Total organic carbon and total inorganic carbon content data of sediment core GeoB18116-2 from Dragon Mound, Alborán Sea, Maria S. Merian cruise MSM36, PANGAEA [data set], <https://doi.org/10.1594/PANGAEA.971862>, 2025f.
- Greiffenhagen, L., Titschack, J., Wienberg, C., Wang, H., Hebbeln, D., Timann, C., and Lemke, A.-J.: CT raw data (DICOM format) of sediment core GeoB18116-2 from Dragon Mound, Alborán Sea, Maria S. Merian cruise MSM36, PANGAEA [data set], <https://doi.org/10.1594/PANGAEA.973154>, 2025g.
- Greiffenhagen, L., Titschack, J., Wienberg, C., Wang, H., and Hebbeln, D.: Processed CT image-based volume data of sediment core GeoB18116-2 from Dragon Mound, Alborán Sea, Maria S. Merian cruise MSM36, PANGAEA [data set], <https://doi.org/10.1594/PANGAEA.971900>, 2025h.
- Hanz, U., Wienberg, C., Hebbeln, D., Duineveld, G., Lavaley, M., Juva, K., Dullo, W.-C., Freiwald, A., Tamborrino, L., Reichart, G.-J., Flögel, S., and Mienis, F.: Environmental factors influencing benthic communities in the oxygen minimum zones on the Angolan and Namibian margins, *Biogeosciences*, 16, 4337–4356, <https://doi.org/10.5194/bg-16-4337-2019>, 2019.
- Hayes, D. R., Schroeder, K., Poulain, P.-M., Testor, P., Mortier, L., Bosse, A., and du Madron, X.: Review of the Circulation and Characteristics of Intermediate Water Masses of the Mediterranean: Implications for Cold-Water Coral Habitats, in: *Mediterranean Cold-Water Corals: Past, Present and Future Coral Reefs of the World*, 195–211, [https://doi.org/10.1007/978-3-319-91608-8\\_18](https://doi.org/10.1007/978-3-319-91608-8_18), 2019.
- Hebbeln, D.: Highly Variable Submarine Landscapes in the Alborán Sea Created by Cold-Water Corals, in: *Mediterr. Cold-Water Corals: Past, Present and Future*, edited by: Orejas, C. and Jimenez, C., Vol. 9, *Coral Reefs of the World*, [https://doi.org/10.1007/978-3-319-91608-8\\_8](https://doi.org/10.1007/978-3-319-91608-8_8), 2019.
- Hebbeln, D. and Gaide, S.: MSM36 raw data of EM122 multi-beam echosounder (bathymetry, beam time series & water column data) for the Alboran Sea, MARUM – Center for Marine Environmental Sciences, University Bremen, PANGAEA [data set], <https://doi.org/10.1594/PANGAEA.895349>, 2018.
- Hebbeln, D., Wienberg, C., Beuck, L., Freiwald, A., Wintersteller, P., and cruise participants: Report and preliminary results of RV POSEIDON Cruise POS 385 “Cold-Water Corals of the Alboran Sea (western Mediterranean Sea)”, Faro – Toulon, 29 May–16 June 2009, Bremen, Germany, <http://nbn-resolving.de/urn:nbn:de:gbv:46-ep000106508> (last access: 29 April 2025), 2009.
- Hebbeln, D., Wienberg, C., Bartels, M., Bergenthal, M., Frank, N., Gaide, S., Henriot, J. P., Kaszemeik, K., Klar, S., Klein, T., Krenzel, T., Kuhnert, M., Meyer-Schack, B., Noorlander, C., Reuter, M., Rosiak, U., Schmidt, W., Seeba, H., Seiter, C., Strange, N., Terhzaz, L., and Van Rooij, D.: MoccoMeBo: Climate-driven development of Moroccan cold-water coral mounds revealed by MeBo-drilling: Atlantic vs. Mediterranean settings, [https://doi.org/10.2312/cr\\_msm36](https://doi.org/10.2312/cr_msm36), 2015.
- Hebbeln, D., Van Rooij, D. and Wienberg, C.: Good neighbours shaped by vigorous currents: Cold-water coral mounds and contourites in the North Atlantic, *Mar. Geol.*, 378, 171–185, <https://doi.org/10.1016/j.margeo.2016.01.014>, 2016.
- Hebbeln, D., Bender, M., Gaide, S., Titschack, J., Vandorpe, T., Van Rooij, D., Wintersteller, P., and Wienberg, C.: Thousands of cold-water coral mounds along the Moroccan Atlantic continental margin: Distribution and morphometry, *Mar. Geol.*, 411, 51–61, <https://doi.org/10.1016/j.margeo.2019.02.001>, 2019.
- Henry, L.-A. and Roberts, J. M.: Biodiversity and ecological composition of macrobenthos on cold-water coral mounds and adjacent off-mound habitat in the bathyal Porcupine Seabight, NE Atlantic, *Deep Sea Res. Oceanogr. Res. Pap.*, 54, 654–672, <https://doi.org/10.1016/j.dsr.2007.01.005>, 2007.
- Henry, L.-A. and Roberts, J. M.: Global biodiversity in cold-water coral reef ecosystems, in: *Marine Animal Forests*, edited by: Rossi, S., Bramanti, L., Gori, A., and Orejas, C., Springer, 235–256, [https://doi.org/10.1007/978-3-319-21012-4\\_6](https://doi.org/10.1007/978-3-319-21012-4_6), 2017.
- Howard, J., Sutton-Grier, A., Herr, D., Kleypas, J., Landis, E., McLeod, E., Pidgeon, E., and Simpson, S.: Clarifying the role of coastal and marine systems in climate mitigation, *Front. Ecol. Environ.*, 15, 42–50, <https://doi.org/10.1002/fee.1451>, 2017.
- Huvenne, V. A. I., Van Rooij, D., De Mol, B., Thierens, M., O’Donnell, R., and Foubert, A.: Sediment dynamics and palaeo-environmental context at key stages in the Challenger cold-water coral mound formation: Clues from sediment deposits at the mound base, *Deep-Sea Res. I*, 56, 2263–2280, <https://doi.org/10.1016/j.dsr.2009.08.003>, 2009.

- IODP: Depth Scales Terminology, Ver. 2.0. <https://www.iodp.org/policies-and-guidelines/142-iodp-depth-scales-terminology-april-2011/file> (last access: 29 April 2025), 2011.
- James, K., Macreadie, P. I., Burdett, H. L., Davies, I., and Kamenos, N. A.: It's time to broaden what we consider a 'blue carbon ecosystem', *Glob. Change Biol.*, 30, e17261, <https://doi.org/10.1111/gcb.17261>, 2024.
- Johnson, B. J., Moore, K. A., Lehmann, C., Bohlen, C., and Brown, T. A.: Middle to late Holocene fluctuations of C<sub>3</sub> and C<sub>4</sub> vegetation in a Northern New England Salt Marsh, Sprague Marsh, Phippsburg Maine, *Org. Geochem.*, 38, 394–403, <https://doi.org/10.1016/j.orggeochem.2006.06.006>, 2007.
- Karlson, A. M., Nascimento, F. J., Naslund, J., and Elm-gren, R.: Higher diversity of deposit-feeding macrofauna enhances phytodetritus processing, *Ecology*, 91, 1414–1423, <https://doi.org/10.1890/09-0660.1>, 2010.
- Kiriakoulakis, K., Bett, B. J., White, M., and Wolff, G. A.: Organic biogeochemistry of the Darwin Mounds, a deep-water coral ecosystem, of the NE Atlantic, *Deep-Sea Res. I*, 51, 1937–1954, <https://doi.org/10.1016/j.dsr.2004.07.010>, 2004.
- Kiriakoulakis, K., Freiwald, A., Fisher, E., and Wolff, G. A.: Organic matter quality and supply to deep-water coral/mound systems of the NW European Continental Margin, *Int. J. Earth Sci.*, 96, 159–170, <https://doi.org/10.1007/s00531-006-0078-6>, 2007.
- Korpanty, C. A., Hoffman, L., da Costa Portillo-Ramos, R., Titschack, J., Wienberg, C., and Hebbeln, D.: Decline in cold-water coral growth promotes molluscan diversity: A paleontological perspective from a cold-water coral mound in the western Mediterranean Sea, *Front. Mar. Sci.*, 9, 895946, <https://doi.org/10.3389/fmars.2022.895946>, 2023.
- Langner, M. and Mulitza, S.: Technical note: PaleoDataView – a software toolbox for the collection, homogenization and visualization of marine proxy data, *Clim. Past*, 15, 2067–2072, <https://doi.org/10.5194/cp-15-2067-2019>, 2019.
- Lindberg, B. and Mienert, J.: Postglacial carbonate production by cold-water corals on the Norwegian Shelf and their role in the global carbonate budget, *Geology*, 33, 537–540, <https://doi.org/10.1130/g21577.1>, 2005.
- Lisiecki, L. E. and Raymo, M. E.: A Pliocene-Pleistocene stack of 57 globally distributed benthic  $\delta^{18}\text{O}$  records, *Paleoceanography*, 20, PA1003, <https://doi.org/10.1029/2004pa001071>, 2005.
- Lo Iacono, C., Gràcia, E., Ranero, C. R., Emelianov, M., Huvenne, V. A. I., Bartolomé, R., Booth-Rea, G., Prades, J., Ambroso, S., Dominguez, C., Grinyó, J., Rubio, E., and Torrent, J.: The West Melilla cold water coral mounds, Eastern Alboran Sea: Morphological characterization and environmental context, *Deep-Sea Res. II*, 99, 316–326, <https://doi.org/10.1016/j.dsr2.2013.07.006>, 2014.
- Lougheed, B. C. and Obrochta, S. P.: A Rapid, Deterministic Age-Depth Modeling Routine for Geological Sequences With Inherent Depth Uncertainty, *Paleoceanogr. Paleoclimatol.*, 34, 122–133, <https://doi.org/10.1029/2018pa003457>, 2019.
- Maier, S. R., Kutti, T., Bannister, R. J., Fang, J. K., van Breugel, P., van Rijswijk, P., and van Oevelen, D.: Recycling pathways in cold-water coral reefs: Use of dissolved organic matter and bacteria by key suspension feeding taxa, *Sci. Rep.*, 10, 9942, <https://doi.org/10.1038/s41598-020-66463-2>, 2020.
- Maier, S. R., Brooke, S., De Clippele, L. H., de Froe, E., van der Kaaden, A.-S., Kutti, T., Mienis, F., and van Oevelen, D.: On the paradox of thriving cold-water coral reefs in the food-limited deep sea, *Biol. Rev.*, 98, 1298–1316, <https://doi.org/10.1111/brv.12976>, 2023.
- Masqué, P., Fabres, J., Canals, M., Sanchez-Cabeza, J. A., Sanchez-Vidal, A., Cacho, I., Calafat, A. M., and Bruach, J. M.: Accumulation rates of major constituents of hemipelagic sediments in the deep Alboran Sea: a centennial perspective of sedimentary dynamics, *Mar. Geol.*, 193, 207–233, [https://doi.org/10.1016/S0025-3227\(02\)00593-5](https://doi.org/10.1016/S0025-3227(02)00593-5), 2003.
- Michel, J., Laugié, M., Pohl, A., Lanteaume, C., Masse, J.-P., Donnadieu, Y., and Borgomano, J.: Marine carbonate factories: a global model of carbonate platform distribution, *Int. J. Earth Sci.*, 108, 1773–1792, <https://doi.org/10.1007/s00531-019-01742-6>, 2019.
- Mienis, F., de Stigter, H. C., White, M., Duineveld, G., de Haas, H., and van Weering, T. C. E.: Hydrodynamic controls on cold-water coral growth and carbonate-mound development at the SW and SE Rockall Trough Margin, NE Atlantic Ocean, *Deep-Sea Res. I*, 54, 1655–1674, <https://doi.org/10.1016/j.dsr.2007.05.013>, 2007.
- Milliman, J. D.: Precipitation and Cementation of Deep-Sea Carbonate Sediments, in: *Deep-Sea Sediments: Physical and Mechanical Properties*, edited by: Inderbitzen, A. L., Springer US, Boston, MA, 463–476, [https://doi.org/10.1007/978-1-4684-2754-7\\_23](https://doi.org/10.1007/978-1-4684-2754-7_23), 1974.
- Milliman, J. D.: Production and accumulation of calcium carbonate in the ocean: Budget of a nonsteady state, *Global Biogeochem. Cy.*, 7, 927–957, <https://doi.org/10.1029/93GB02524>, 1993.
- Millot, C.: Circulation in the western Mediterranean Sea, *J. Mar. Syst.*, 20, 423–442, [https://doi.org/10.1016/S0924-7963\(98\)00078-5](https://doi.org/10.1016/S0924-7963(98)00078-5), 1999.
- Mohn, C., Rengstorf, A., White, M., Duineveld, G., Mienis, F., Soetaert, K., and Grehan, A.: Linking benthic hydrodynamics and cold-water coral occurrences: A high-resolution model study at three cold-water coral provinces in the NE Atlantic, *Prog. Oceanogr.*, 122, 92–104, <https://doi.org/10.1016/j.pocean.2013.12.003>, 2014.
- Morán, X. A. G. and Estrada, M.: Short-term variability of photosynthetic parameters and particulate and dissolved primary production in the Alboran Sea (SW Mediterranean), *Mar. Ecol. Prog. Ser.*, 212, 53–67, <https://doi.org/10.3354/meps212053>, 2001.
- O'Mara, N. A. and Dunne, J. P.: Hot Spots of Carbon and Alkalinity Cycling in the Coastal Oceans, *Sci. Rep.*, 9, 4434, <https://doi.org/10.1038/s41598-019-41064-w>, 2019.
- Orsi, T. H. and Anderson, A. L.: Bulk density calibration for X-ray tomographic analyses of marine sediments, *Geo-Mar. Lett.*, 19, 270–274, <https://doi.org/10.1007/s003670050118>, 1999.
- Orsi, T. H., Edwards, C. M., and Anderson, A. L.: X-ray computed tomography: a nondestructive method for quantitative analysis of sediment cores, *J. Sediment. Res.*, 64, 3, <https://doi.org/10.1306/D4267E74-2B26-11D7-8648000102C1865D>, 1994.
- Paradis, S., Nakajima, K., Van der Voort, T. S., Gies, H., Wildberger, A., Blattmann, T. M., Bröder, L., and Eglinton, T. I.: The Modern Ocean Sediment Archive and Inventory of Carbon (MOSAIC): version 2.0, *Earth Syst. Sci. Data*, 15, 4105–4125, <https://doi.org/10.5194/essd-15-4105-2023>, 2023.

- Pirlet, H., Colin, C., Thierens, M., Latruwe, K., Van Rooij, D., Foubert, A., Frank, N., Blamart, D., Huvenne, V. A. I., Swennen, R., Vanhaecke, F., and Henriët, J.-P.: The importance of the terrigenous fraction within a cold-water coral mound: A case study, *Mar. Geol.*, 282, 13–25, <https://doi.org/10.1016/j.margeo.2010.05.008>, 2011.
- Portilho-Ramos, R. D. C., Titschack, J., Wienberg, C., Sicha Rojas, M. G., Yokoyama, Y., and Hebbeln, D.: Major environmental drivers determining life and death of cold-water corals through time, *PLoS Biol.*, 20, e3001628, <https://doi.org/10.1371/journal.pbio.3001628>, 2022.
- Puig, P., Palanques, A., Guillén, J., and El Khatab, M.: Role of internal waves in the generation of nepheloid layers on the northwestern Alboran slope: Implications for continental margin shaping, *J. Geophys. Res.-Oceans*, 109, C09011, <https://doi.org/10.1029/2004jc002394>, 2004.
- Reijmer, J. J. G.: Marine carbonate factories: Review and update, *Sedimentology*, 68, 1729–1796, <https://doi.org/10.1111/sed.12878>, 2021.
- Reimer, P. J., Austin, W. E. N., Bard, E., Bayliss, A., Blackwell, P. G., Bronk Ramsey, C., Butzin, M., Cheng, H., Edwards, R. L., Friedrich, M., Grootes, P. M., Guilderson, T. P., Hajdas, I., Heaton, T. J., Hogg, A. G., Hughen, K. A., Kromer, B., Manning, S. W., Muscheler, R., Palmer, J. G., Pearson, C., van der Plicht, J., Reimer, R. W., Richards, D. A., Scott, E. M., Southon, J. R., Turney, C. S. M., Wacker, L., Adolphi, F., Büntgen, U., Capano, M., Fahrni, S. M., Fogtmann-Schulz, A., Friedrich, R., Köhler, P., Kudsk, S., Miyake, F., Olsen, J., Reinig, F., Sakamoto, M., Sookdeo, A., and Talamo, S.: The IntCal20 Northern Hemisphere Radiocarbon Age Calibration Curve (0–55 cal kBP), *Radiocarbon*, 62, 725–757, <https://doi.org/10.1017/rdc.2020.41>, 2020.
- Ridgwell, A. and Zeebe, R.: The role of the global carbonate cycle in the regulation and evolution of the Earth system, *Earth Planet. Sci. Lett.*, 234, 299–315, <https://doi.org/10.1016/j.epsl.2005.03.006>, 2005.
- Roberts, J. M., Freiwald, A., Wheeler, A., and Cairns, S.: *Cold-Water Corals*, Cambridge Univ. Press, <https://doi.org/10.1017/cbo9780511581588.005>, 2009.
- Rossi, S. and Rizzo, L.: Marine Animal Forests as Carbon Immobilizers or Why We Should Preserve These Three-Dimensional Alive Structures, in: *Perspect. Mar. Anim. Forests World*, edited by: Rossi, S. and Bramanti, L., 333–400, [https://doi.org/10.1007/978-3-030-57054-5\\_11](https://doi.org/10.1007/978-3-030-57054-5_11), 2020.
- Roulet, N. T., Lafleur, P. M., Richard, P. J. H., Moore, T. R., Humphreys, E. R., and Bubier, J.: Contemporary carbon balance and late Holocene carbon accumulation in a northern peatland, *Global Change Biol.*, 13, 397–411, <https://doi.org/10.1111/j.1365-2486.2006.01292.x>, 2007.
- Samper-Villarreal, J., Mumby, P. J., Saunders, M. I., Barry, L. A., Zawadzki, A., Heijnis, H., Morelli, G., and Lovelock, C. E.: Vertical accretion and carbon burial rates in subtropical seagrass meadows increased following anthropogenic pressure from European colonisation, *Estuar. Coast. Shelf Sci.*, 202, 40–53, <https://doi.org/10.1016/j.ecss.2017.12.006>, 2018.
- Sánchez-Garrido, J. C. and Nadal, I.: The Alboran Sea circulation and its biological response: A review, *Front. Mar. Sci.*, 9, 933390, <https://doi.org/10.3389/fmars.2022.933390>, 2022.
- Sanchez-Vidal, A., Calafat, A., Canals, M., Frigola, J., and Fabres, J.: Particle fluxes and organic carbon balance across the Eastern Alboran Sea (SW Mediterranean Sea), *Cont. Shelf Res.*, 25, 609–628, <https://doi.org/10.1016/j.csr.2004.11.004>, 2005.
- Schlager, W.: The paradox of drowned reefs and carbonate platforms, *GSA Bull.*, 92, 197–211, [https://doi.org/10.1130/0016-7606\(1981\)92<197:TPODRA>2.0.CO;2](https://doi.org/10.1130/0016-7606(1981)92<197:TPODRA>2.0.CO;2), 1981.
- Schlager, W.: Sedimentation rates and growth potential of tropical, cool-water and mud-mound carbonate systems, *Geol. Soc. Lond. Spec. Publ.*, 178, 217–227, <https://doi.org/10.1144/GSL.SP.2000.178.01.14>, 2000.
- Schlager, W.: Benthic carbonate factories of the Phanerozoic, *Int. J. Earth Sci.*, 92, 445–464, <https://doi.org/10.1007/s00531-003-0327-x>, 2003.
- Schmitz, O. J., Raymond, P. A., Estes, J. A., Kurz, W. A., Holtgrieve, G. W., Ritchie, M. E., Schindler, D. E., Spivak, A. C., Wilson, R. W., Bradford, M. A., Christensen, V., Deegan, L., Smetacek, V., Vanni, M. J., and Wilmers, C. C.: Animating the Carbon Cycle, *Ecosystems*, 17, 344–359, <https://doi.org/10.1007/s10021-013-9715-7>, 2014.
- Schmitz, O. J., Wilmers, C. C., Leroux, S. J., Doughty, C. E., Atwood, T. B., Galetti, M., Davies, A. B., and Goetz, S. J.: Animals and the zoogeography of the carbon cycle, *Science*, 362, 6419, <https://doi.org/10.1126/science.aar3213>, 2018.
- Shipboard Scientific Party: Site 979, in: *Leg 161, Proc. ODP, Init. Repts.*, edited by: Comas, M. C., Zahn, R., Klaus, A., et al., College Station, TX (Ocean Drilling Program), 389–426, <https://doi.org/10.2973/odp.proc.ir.161.109.1996>, 1996.
- Smith, S. V. and Mackenzie, F. T.: The Role of CaCO<sub>3</sub> Reactions in the Contemporary Oceanic CO<sub>2</sub> Cycle, *Aquat. Geochem.*, 22, 153–175, <https://doi.org/10.1007/s10498-015-9282-y>, 2016.
- Soetaert, K., Mohn, C., Rengstorf, A., Grehan, A., and van Oevelen, D.: Ecosystem engineering creates a direct nutritional link between 600-m deep cold-water coral mounds and surface productivity, *Sci. Rep.*, 6, 35057, <https://doi.org/10.1038/srep35057>, 2016.
- Stalder, C., El Kateb, A., Vertino, A., Rüggeberg, A., Camozzi, O., Pirkenseer, C. M., Spangenberg, J. E., Hajdas, I., Van Rooij, D., and Spezzaferri, S.: Large-scale paleoceanographic variations in the western Mediterranean Sea during the last 34,000 years: From enhanced cold-water coral growth to declining mounds, *Mar. Micropaleontol.*, 143, 46–62, <https://doi.org/10.1016/j.marmicro.2018.07.007>, 2018.
- Stalling, D., Westerhoff, M., and Hege, H.-C.: Amira: a highly interactive system for visual data analysis, in: *Visualization Handbook*, edited by: Hansen, C. D. and Johnson, C. R., Butterworth-Heinemann, 749–767, <https://doi.org/10.1016/B978-012387582-2/50040-X>, 2005.
- Strong, J. A., Andonegi, E., Bizsel, K. C., Danovaro, R., Elliott, M., Franco, A., Garcés, E., Little, S., Mazik, K., Moncheva, S., Papadopoulou, N., Patrício, J., Queirós, A. M., Smith, C., Stefanova, K., and Solaun, O.: Marine biodiversity and ecosystem function relationships: The potential for practical monitoring applications, *Estuar. Coast. Shelf Sci.*, 161, 46–64, <https://doi.org/10.1016/j.ecss.2015.04.008>, 2015.
- Tamborrino, L., Wienberg, C., Titschack, J., Wintersteller, P., Mienis, F., Schröder-Ritzrau, A., Freiwald, A., Orejas, C., Dullo, W.-C., Haberkern, J., and Hebbeln, D.: Mid-Holocene extinction of cold-water corals on the Namibian shelf steered by the Benguela oxygen minimum zone, *Geology*, 47, 1185–1188, <https://doi.org/10.1130/g46672.1>, 2019.

- Tamborrino, L., Titschack, J., Wienberg, C., Purkis, S., Eberli, G. P., and Hebbeln, D.: Spatial distribution and morphometry of the Namibian coral mounds controlled by the hydrodynamic regime and outer-shelf topography, *Front. Mar. Sci.*, 9, 877616, <https://doi.org/10.3389/fmars.2022.877616>, 2022.
- Thiem, Ø., Ravagnan, E., Fosså, J. H., and Berntsen, J.: Food supply mechanisms for cold-water corals along a continental shelf edge, *J. Mar. Syst.*, 60, 207–219, <https://doi.org/10.1016/j.jmarsys.2005.12.004>, 2006.
- Titschack, J., Thierens, M., Dorschel, B., Schulbert, C., Freiwald, A., Kano, A., Takashima, C., Kawagoe, N., and Li, X.: Carbonate budget of a cold-water coral mound (Challenger Mound, IODP Exp. 307), *Mar. Geol.*, 259, 36–46, <https://doi.org/10.1016/j.margeo.2008.12.007>, 2009.
- Titschack, J., Baum, D., De Pol-Holz, R., López Correa, M., Forster, N., Flögel, S., Hebbeln, D., Freiwald, A., and Riegl, B.: Aggradation and carbonate accumulation of Holocene Norwegian cold-water coral reefs, *Sedimentology*, 62, 1873–1898, <https://doi.org/10.1111/sed.12206>, 2015.
- Titschack, J., Fink, H. G., Baum, D., Wienberg, C., Hebbeln, D., and Freiwald, A.: Mediterranean cold-water corals – an important regional carbonate factory?, *The Depositional Record*, 2, 74–96, <https://doi.org/10.1002/dep2.14>, 2016.
- van der Kaaden, A., Mohn, C., Gerkema, T., Maier, S. R., de Froe, E., van de Koppel, J., Rietkerk, M., Soetaert, K., and van Oevelen, D.: Feedbacks between hydrodynamics and cold-water coral mound development, *Deep-Sea Res. I*, 178, 103641, <https://doi.org/10.1016/j.dsr.2021.103641>, 2021.
- van Oevelen, D., Duineveld, G., Lavaleye, M., Mienis, F., Soetaert, K., and Heip, C. H. R.: The cold-water coral community as hotspot of carbon cycling on continental margins: A food-web analysis from Rockall Bank (northeast Atlantic), *Limnol. Oceanogr.*, 54, 1829–1844, <https://doi.org/10.4319/lo.2009.54.6.1829>, 2009.
- Van Rooij, D., Hebbeln, D., Comas, M. C., Vandorpe, T., Delivet, S., and Scientists, M. S.: EUROFLEETS Cruise Summary Report GATEWAY. The Mediterranean-Atlantic Gateway Code: The Late Pleistocene Carbonate Mound Record. R/V Marion Dufresne, Cruise No. 194, 10–20 June 2013, Cadiz (Spain) – Lisbon (Portugal), <https://doi.org/10.17600/13200130>, 2013.
- Wang, H., Lo Iacono, C., Wienberg, C., Titschack, J., and Hebbeln, D.: Cold-water coral mounds in the southern Alboran Sea (western Mediterranean Sea): Internal waves as an important driver for mound formation since the last deglaciation, *Mar. Geol.*, 412, 1–18, <https://doi.org/10.1016/j.margeo.2019.02.007>, 2019.
- Wang, H., Titschack, J., Wienberg, C., Korpanty, C., and Hebbeln, D.: The Importance of Ecological Accommodation Space and Sediment Supply for Cold-Water Coral Mound Formation, a Case Study From the Western Mediterranean Sea, *Front. Mar. Sci.*, 8, 760909, <https://doi.org/10.3389/fmars.2021.760909>, 2021.
- Wang, H., Titschack, J., Wienberg, C., Korpanty, C., and Hebbeln, D.: The importance of ecological accommodation space and sediment supply for cold-water coral mound formation, a case study from the Western Mediterranean Sea, PANGAEA [data set], in review, <https://doi.org/10.1594/PANGAEA.941018>, 2025.
- Wehrmann, L. M., Knab, N. J., Pirlet, H., Unnithan, V., Wild, C., and Ferdelman, T. G.: Carbon mineralization and carbonate preservation in modern cold-water coral reef sediments on the Norwegian shelf, *Biogeosciences*, 6, 663–680, <https://doi.org/10.5194/bg-6-663-2009>, 2009.
- Wheeler, A. J., Beyer, A., Freiwald, A., de Haas, H., Huvenne, V. A. I., Kozachenko, M., Olu-Le Roy, K., and Opperbecke, J.: Morphology and environment of cold-water coral carbonate mounds on the NW European margin, *Int. J. Earth Sci.*, 96, 37–56, <https://doi.org/10.1007/s00531-006-0130-6>, 2007.
- Wheeler, A. J., Kozachenko, M., Masson, D. G., and Huvenne, V. A. I.: Influence of benthic sediment transport on cold-water coral bank morphology and growth: the example of the Darwin Mounds, north-east Atlantic, *Sedimentology*, 55, 1875–1887, <https://doi.org/10.1111/j.1365-3091.2008.00970.x>, 2008.
- Wienberg, C.: A Deglacial Cold-Water Coral Boom in the Alborán Sea: From Coral Mounds and Species Dominance, *Mediterr. Cold-Water Corals: Past, Present and Future Coral Reefs of the World*, 57–60, [https://doi.org/10.1007/978-3-319-91608-8\\_7](https://doi.org/10.1007/978-3-319-91608-8_7), 2019.
- Wienberg, C. and Titschack, J.: Framework-Forming Scleractinian Cold-Water Corals Through Space and Time: A Late Quaternary North Atlantic Perspective, in: *Marine Animal Forests*, edited by: Rossi, S., Bramanti, L., Gori, A., and Orejas, C., 699–732, [https://doi.org/10.1007/978-3-319-17001-5\\_16-1](https://doi.org/10.1007/978-3-319-17001-5_16-1), 2017.
- Wienberg, C., Titschack, J., Freiwald, A., Frank, N., Lundälv, T., Taviani, M., Beuck, L., Schröder-Ritzrau, A., Kregel, T., and Hebbeln, D.: The giant Mauritanian cold-water coral mound province: Oxygen control on coral mound formation, *Quat. Sci. Rev.*, 185, 135–152, <https://doi.org/10.1016/j.quascirev.2018.02.012>, 2018.
- Wienberg, C., Kregel, T., Frank, N., Wang, H., Van Rooij, D., and Hebbeln, D.: Cold-water coral mounds in the western Mediterranean Sea: New insights into their initiation and development since the Mid-Pleistocene in response to changes of African hydroclimate, *Quat. Sci. Rev.*, 293, 107723, <https://doi.org/10.1016/j.quascirev.2022.107723>, 2022.
- Wienberg, C., Freiwald, A., Frank, N., Mienis, F., Titschack, J., Orejas, C., and Hebbeln, D.: Cold-Water Coral Reefs in the Oxygen Minimum Zones Off West Africa, *Cold-Water Coral Reefs of the World*, 199–235, [https://doi.org/10.1007/978-3-031-40897-7\\_8](https://doi.org/10.1007/978-3-031-40897-7_8), 2023.
- Wood, M., Hayes, C. T., and Paytan, A.: Global Quaternary Carbonate Burial: Proxy- and Model-Based Reconstructions and Persisting Uncertainties, *Ann. Rev. Mar. Sci.*, 15, 277–302, <https://doi.org/10.1146/annurev-marine-031122-031137>, 2023.
- Yin, S., Hernández-Molina, F. J., Fan, W., and Li, J.: Efficient organic carbon burial by bottom currents in the ocean: A potential role in climate modulation, *Geophys. Res. Lett.*, 51, e2024GL109444, <https://doi.org/10.1029/2024GL109444>, 2024.